INL/EXT-16-40305
Revision 0

Status on the Component Models Developed in the Modelica Framework: High-Temperature Steam Electrolysis Plant & Gas Turbine Power Plant

Jong Suk Kim
Michael McKellar
Shannon M. Bragg-Sitton
Richard D. Boardman

October 2016

The INL is a U.S. Department of Energy National Laboratory
operated by Battelle Energy Alliance

DISCLAIMER

This information was prepared as an account of work sponsored by an agency of the U.S. Government. Neither the U.S. Government nor any agency thereof, nor any of their employees, makes any warranty, expressed or implied, or assumes any legal liability or responsibility for the accuracy, completeness, or usefulness, of any information, apparatus, product, or process disclosed, or represents that its use would not infringe privately owned rights. References herein to any specific commercial product, process, or service by trade name, trade mark, manufacturer, or otherwise, does not necessarily constitute or imply its endorsement, recommendation, or favoring by the U.S. Government or any agency thereof. The views and opinions of authors expressed herein do not necessarily state or reflect those of the U.S. Government or any agency thereof.

INL/EXT-16-40305
Revision 0

Status on the Component Models Developed in the Modelica Framework: High-Temperature Steam Electrolysis Plant & Gas Turbine Power Plant

Jong Suk Kim
Michael McKellar
Shannon M. Bragg-Sitton
Richard D. Boardman

October 2016

Idaho National Laboratory
Idaho Falls, Idaho 83415

http://www.inl.gov

Prepared for the
U.S. Department of Energy
Office of Nuclear Energy
Under DOE Idaho Operations Office
Contract DE-AC07-05ID14517

ABSTRACT

This report has been prepared as part of an effort to design and build a modeling and simulation (M&S) framework to assess the economic viability of a nuclear-renewable hybrid energy system (N-R HES). In order to facilitate dynamic M&S of such an integrated system, research groups in multiple national laboratories have been developing various subsystems as dynamic physics-based components using the Modelica programming language. In fiscal year (FY) 2015, Idaho National Laboratory (INL) performed a dynamic analysis of two region-specific N-R HES configurations, including the gas-to-liquid (natural gas to Fischer-Tropsch synthetic fuel) and brackish water reverse osmosis desalination plants as industrial processes. In FY 2016, INL has developed two additional subsystems in the Modelica framework: a high-temperature steam electrolysis (HTSE) plant and a gas turbine power plant (GTPP).

HTSE has been proposed as a high priority industrial process to be integrated with a light water reactor (LWR) in an N-R HES. This integrated energy system would be capable of dynamically apportioning thermal and electrical energy (1) to provide responsive generation to the power grid and (2) to produce alternative industrial products (i.e., hydrogen and oxygen) without generating any greenhouse gases. A dynamic performance analysis of the LWR/HTSE integration case was carried out to evaluate the technical feasibility (load-following capability) and safety of such a system operating under highly variable conditions requiring flexible output. To support the dynamic analysis, the detailed dynamic model and control design of the HTSE process, which employs solid oxide electrolysis cells, have been developed to predict the process behavior over a large range of operating conditions. As first-generation N-R HES technology will be based on LWRs, which provide thermal energy at a relatively low temperature, complementary temperature-boosting technology was suggested for integration with the HTSE process that requires higher temperature input. Simulation results involving several case studies show that the suggested control scheme could maintain the controlled variables (including the steam utilization factor, cathode stream inlet composition, and temperatures of the process streams at various locations) within desired limits under various plant operating conditions. The results also indicate that the proposed HTSE plant could provide operational flexibility to participate in energy management at the utility scale by dynamically optimizing the use of excess plant capacity within an N-R HES.

A natural-gas fired GTPP has been proposed as a secondary energy supply to be included in an N-R HES. This auxiliary generator could be used to cover rapid dynamics in grid demand that cannot be met by the remainder of the N-R HES. To evaluate the operability and controllability of the proposed process during transients between load (demand) levels, the dynamic model and control design were developed. Special attention was given to the design of feedback controllers to regulate the power frequency, and exhaust gas and turbine firing temperatures. Several case studies were performed to investigate the system responses to the major disturbance (power load demand) in such a control system. The simulation results show that the performance of the proposed control strategies was satisfactory under each test when the GTPP experienced high rapid variations in the load.

CONTENTS

FIGURES

TABLES

ACRONYMS

ANL	Argonne National Laboratory
CV	Controlled variable
Dymola	Dynamic modeling library
ETH	Electric topping heater
FLR	Flexible load resource
FY	Fiscal year
GTPP	Gas turbine power plant
HDGT	Heavy-duty gas turbine
HES	Hybrid energy system
HTSE	High-temperature steam electrolysis
HX	Heat exchanger
IGV	Inlet guide vane
INL	Idaho National Laboratory
ISO	International organization for standardization
LHV	Lower heating value
LSM	Strontium-doped lanthanum manganite
LVS	Low value selector
LWR	Light water reactor
M&S	Modeling and simulation
MSL	Modelica standard library
MV	Manipulated variable
N-R HES	Nuclear-renewable hybrid energy system
ORNL	Oak Ridge National Laboratory
PI	Proportional-integral
PV	Photovoltaic
RAVEN	Risk Analysis Virtual Environment
ScSZ	Scandia-stabilized zirconia
SOEC	Solid oxide electrolysis cell
SOFC	Solid oxide fuel cell
SU	Steam utilization
TCV	Temperature control valve
VEL	Variable electrical load
YSZ	Yttria-stabilized zirconia

Status on the Component Models Developed in the Modelica Framework: High-Temperature Steam Electrolysis Plant & Gas Turbine Power Plant

1. INTRODUCTION

A nuclear-renewable hybrid energy system (N-R HES) is a conceptual system that could lead to more efficient utilization of clean energy generation sources, including renewable and nuclear options, to meet both grid demand, and thermal and/or electrical energy needs in the industrial sectors. This integrated energy system stores and/or utilizes excess thermal and electrical energy at times of reduced grid demand and/or increased renewable penetration (which results in a reduced net load[1]) to produce the alternative industrial product(s), while simultaneously providing responsive generation to the power grid [1, 2].

Idaho National Laboratory (INL) has identified two region-specific N-R HES configurations in West Texas and Arizona for preliminary technical and operational economic analysis [3-5]. The first configuration employs a nuclear plant and a series of wind turbines to produce electricity and convert carbon resources (natural gas) to synthetic liquid fuels (gasoline and diesel) using excess thermal capacity. The second configuration employs a nuclear plant and solar photovoltaic (PV) stations for energy generation, and yields electricity to meet grid demand and to produce fresh water via reverse osmosis desalination using excess electrical capacity. Both systems have been implemented in Modelica [6].

An effort to design and build a modeling and simulation (M&S) framework to assess the economic viability of an N-R HES was undertaken in fiscal year (FY) 2015 [7]. As part of this effort, INL has been developing advanced M&S tools and capabilities to conduct detailed systems-level design optimization for integrated energy systems based on defined technical and economic performance parameters (figures of merit). Risk Analysis Virtual Environment (RAVEN), a flexible and multi-purpose statistical analysis framework developed at INL [8], has been chosen as a driver for hybrid energy system (HES) design optimization. RAVEN runs the optimization by varying selected parameters (i.e., perturbing input parameters in the system model), running the Modelica system model and collecting the resulting outputs, and determining the next optimization step [9].

Research groups from three national laboratories, namely Argonne National Laboratory (ANL), Oak Ridge National Laboratory (ORNL), and INL, have been developing various Modelica component models that comprise the N-R HES model(s). Figure 1 presents a generic layout of an N-R HES (i.e., a tightly coupled HES[2]) under development in the Modelica framework.

[1] Net load is the remaining demand that must be met by conventional generation sources after variable generation is subtracted from the total load (demand) [1].

[2] Tightly Coupled HES: Nuclear renewable generation sources and the industrial process(es) are directly integrated behind the grid and co-controlled, such that there is a single connection point to the grid and a single financial entity managing the HES (i.e., profitability of the HES is optimized for the integrated system rather than for each system independently) [10].

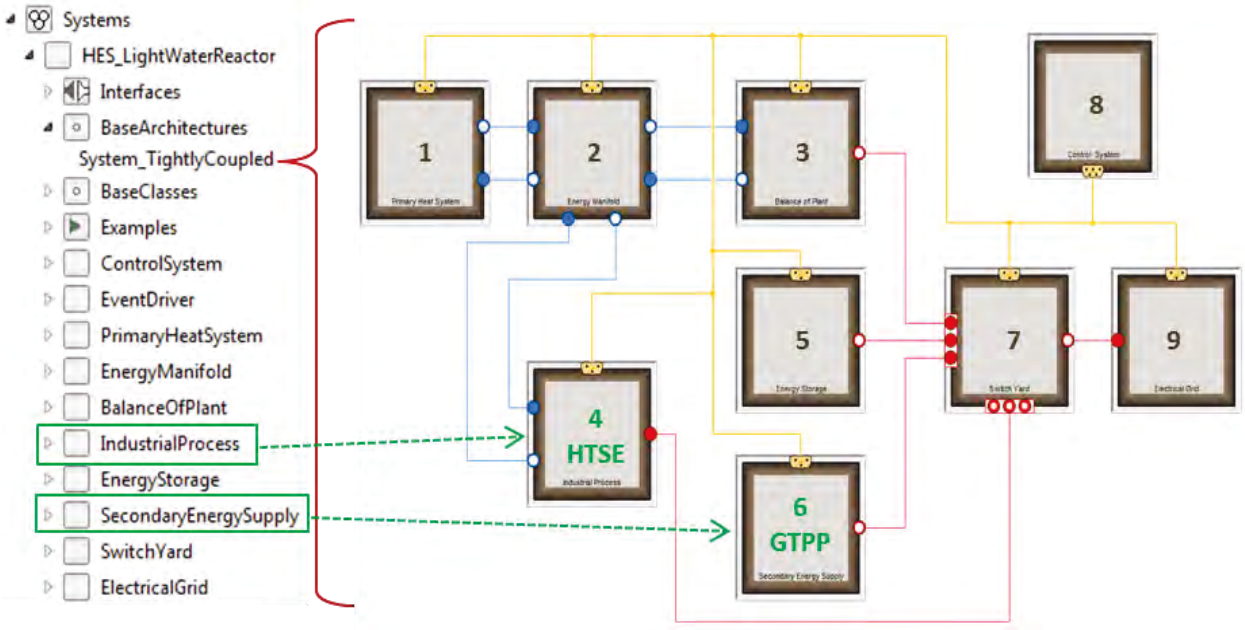

Figure 1. A generic layout of an N-R HES in Modelica. The subsystems developed by INL (shown in green color) are *industrial process* and *secondary energy supply* models.

As illustrated in Figure 1, an N-R HES is divided into nine primary components (subsystems) in an object-oriented fashion that correspond to the modular nature of the system as follows:

1. Primary heat system
2. Energy manifold
3. Balance of plant
4. Industrial process
5. Energy storage
6. Secondary energy supply
7. Switchyard
8. Control system
9. Electric grid

The overall system integration and modeling in Modelica is performed by ORNL with subsystem model contributions from ANL (subsystem 5), INL (subsystems 4 and 6), and ORNL (subsystems 1, 2, 3, and 7). A brief description of the two Modelica subsystem models currently provided by INL is given below; for a description of rest of the subsystems, see Reference [9].

Industrial Process:

High-temperature steam electrolysis (HTSE) is one high priority industrial process that could be integrated within an N-R HES. Steam from the primary heat system (via the energy manifold) provides a portion of the process heat required. The steam will then be sub-cooled and sent back to the energy manifold. The electrical load will be fulfilled by an electricity supply from multiple subsystems, i.e., steam generator, battery, gas turbine, and grid.

Secondary Energy Supply:

A natural gas-fired turbine will be included in an N-R HES as a secondary energy supply. This gas turbine power plant (GTPP) will cover rapid dynamics in grid demand that cannot be met by the remainder of the N-R HES.

1.1 Objective and Approach

The purpose of this report is to provide the current status on component model development in the Modelica framework at INL. Models specifically developed in FY 2016 include an HTSE plant and a GTPP. Numerous tests were carried out to demonstrate the effectiveness of the process design, and control and instrumentation strategies proposed for each subsystem under highly flexible operations. In particular, the technical performance of each subsystem was evaluated in terms of step and load-following responses. In order to assess the load-following capability of the proposed HTSE plant, two types of renewable energy sources (i.e., PV and wind energy) were considered. They were used to replicate the situation, in which an excess electrical power directed to the HTSE process is identical to variable renewable generation with a constant net load imposed by the electric grid. As the emphasis is on a detailed investigation on dynamic performance characteristics of the proposed subsystems under variable operating conditions, mathematical modeling details (i.e., specific governing equations included in each subsystem) are not provided in this report.

1.2 Dynamic Modeling and Simulation

The Modelica [6] modeling language was used with a dynamic modeling library (Dymola) as the M&S environment to construct and simulate the dynamic models of interest. Modelica is primarily a modeling language that allows specification of mathematical models of complex natural or man-made systems, for example, for the purpose of computer simulation of dynamic systems where behavior evolves as a function of time. Modelica is an object-oriented, equation-based programming language, oriented toward computational applications with high complexity requiring high performance. Modelica-related capabilities include a large number of libraries of open-source code for modeling a wide variety of engineering systems. The four most important features that make Modelica both powerful and easy to use, especially for M&S, are [6]:

1. Modelica is primarily based on equations instead of assignment statements. This permits acausal modeling that gives better reuse of classes[3] since equations do not specify a certain data-flow direction. Thus, a Modelica class can adapt to more than one data flow context.
2. Modelica has multi-domain modeling capability, meaning that model components corresponding to physical objects from several different domains, such as electrical, mechanical, thermodynamics, hydraulic, biological, and control applications, can be described and connected.
3. Modelica is an objected-oriented language with a general class concept that unifies classes, generics – known as templates in C++ – and general subtyping into a single language construct. This facilitates reuse of components and evolution of models, resulting in considerably reduced modeling effort.
4. Modelica has a strong software component model, with constructs for creating and connecting components. Thus the language is ideally suited as an architectural description language for complex physical systems and, to some extent, for software systems.

[3] In Modelica, the basic structuring element is a "class," which contains variables (i.e., class attributes representing data).

The level of modeling detail varies from mapping functions to more detailed models (i.e., representative physics-based modeling). In-house developed packages and open-source libraries were utilized to facilitate M&S. In particular, the Modelica standard library (MSL) version 3.2.2 [11] and ThermoPower library version 3.1beta.0 [12] were utilized. Modelica models were implemented using the commercially available Modelica-based M&S environment, i.e., Dymola version 2017. M&S were conducted in compliance with the Modelica code standards (see Appendix A). The plant models were developed on a Dell Precision M4800 with Intel® Core™ i7-4940MX CPU (quad core extreme 3.10 GHz) and with 32.0 GB of RAM (1600 MHz DDR3L).

1.3 Organization

The reminder of this report is organized into two sections. Section 2 presents an overview of the proposed HTSE plant model (including detailed process and control designs) and simulation results involving several case studies with detailed discussion, followed by conclusions. Section 3 is organized in the same fashion as Section 2, but for the proposed GTPP model.

2. HIGH-TEMPERATURE STEAM ELECTROLYSIS PLANT

First-generation N-R HES technology will be based on light water reactors (LWRs) with an initial focus on small modular reactors (defined by a unit size of < 300 MW_e) [10]. These LWRs provide thermal energy at temperatures of approximately 300°C, while the desired temperature for an HTSE process is much higher (i.e., 850°C in the proposed design). To realize the benefits of N-R HESs with an LWR, selection and development of complimentary temperature-boosting technologies and corresponding control design are necessary for integration with an HTSE process. This section is dedicated to detailed process and control designs of the HTSE plant that acts as a flexible load resource (FLR) when integrated within tightly coupled HESs. Simulation results involving several case studies are also provided.

2.1 System Overview

Process details of the HTSE plant model that has been developed to simulate integration of an LWR with the HTSE process, and the associated regulatory control design, are shown in Figure 2. The control design is separately discussed in Section 2.2. Figure 3 shows the top-level model for the HTSE plant implemented in Modelica. As seen in these figures, twelve main subsystems can be identified as follows:

Physical devices:

1. Solid oxide electrolysis cell (SOEC) stacks
2. Heat exchangers (HXs) (or heat recuperators)
3. Electric topping heaters (ETHs)
4. Hydrogen/steam mixer
5. Hydrogen recycle loop
6. Flash drum
7. Switchyard

Control devices:

8. Classical feedback controllers, in particular proportional-integral (PI) controllers (only two are shown in Figures 2 and 3; five are embedded within corresponding subsystems, not shown in Figures 2 and 3)

9. Feedforward controllers (two embedded within corresponding subsystems, not shown in Figures 2 and 3)
10. Temperature control valves (TCVs)
11. Control bus

System-wide setting:

12. System component[4]

Each of these subsystems consists of a number of basic components. A few selected Modelica models for these subsystems are shown in Figures B.1–B.6 in Appendix B. Detailed descriptions of the basic components are beyond the scope of this report.

[4] A system component is needed in each fluid model to provide system-wide settings, such as ambient conditions and overall modeling assumptions. The system settings are propagated to the fluid models using the inner/outer mechanism.

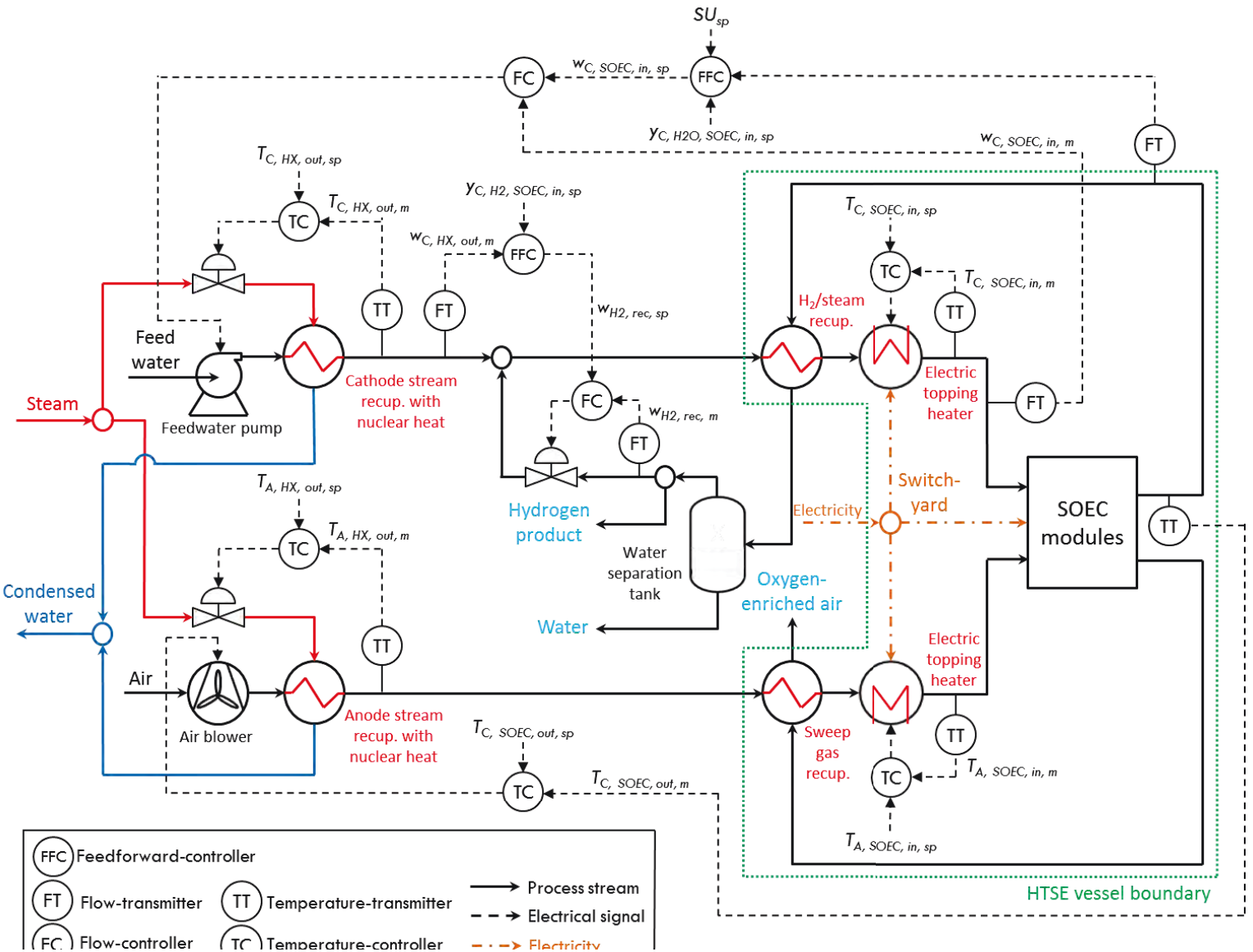
SU_{sp}
FC
$w_{C,\ SOEC,\ in,\ sp}$
FFC
$y_{C,\ H2O,\ SOEC,\ in,\ sp}$
$w_{C,\ SOEC,\ in,\ m}$
FT
$T_{C,\ HX,\ out,\ sp}$
$T_{C,\ HX,\ out,\ m}$
TC
$y_{C,\ H2,\ SOEC,\ in,\ sp}$
$w_{C,\ HX,\ out,\ m}$
FFC
TT
FT
$w_{H2,\ rec,\ sp}$
$T_{C,\ SOEC,\ in,\ sp}$
TC
$T_{C,\ SOEC,\ in,\ m}$
H_2/steam recup.
TT
Feed water
Steam
Feedwater pump
Cathode stream recup. with nuclear heat
FC
$w_{H2,\ rec,\ m}$
FT
Electric topping heater
FT
Switch-yard
Electricity
Hydrogen product
$T_{A,\ HX,\ out,\ sp}$
$T_{A,\ HX,\ out,\ m}$
TC
SOEC modules
TT
Condensed water
Water separation tank
Oxygen-enriched air
Water
TT
Air
Air blower
Anode stream recup. with nuclear heat
Electric topping heater
$T_{C,\ SOEC,\ out,\ sp}$
Sweep gas recup.
TT
$T_{A,\ SOEC,\ in,\ m}$
TC
$T_{C,\ SOEC,\ out,\ m}$
TC
$T_{A,\ SOEC,\ in,\ sp}$
HTSE vessel boundary
FFC Feedforward-controller
FT Flow-transmitter
TT Temperature-transmitter
FC Flow-controller
TC Temperature-controller
Process stream
Electrical signal
Electricity

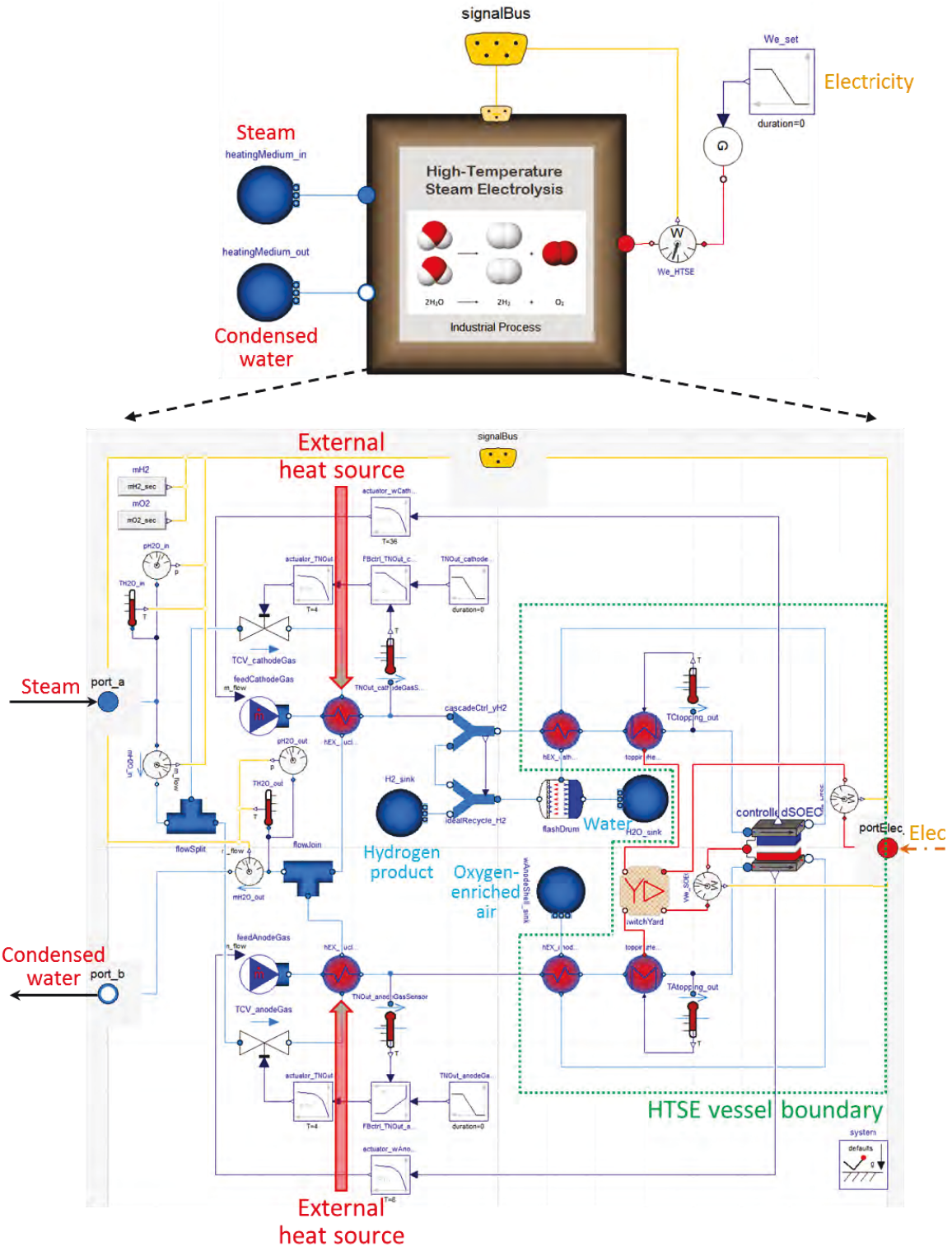

Figure 3. Top-level model for the HTSE plant in Modelica.

HTSE utilizes a combination of thermal energy and electricity to split water into hydrogen (H_2) and oxygen (O_2) in SOECs, which can be seen in simple terms as the reverse operation of solid oxide fuel cells (SOFCs). Figure 4 shows a cross-section of a planar "SOEC stack" (referred to as an electrolyzer) considered in this report. The cathode-supported cell consists of a three-layer solid structure (composed of porous cathode, electrolyte, and porous anode) and an interconnect (separator) plate [13]. An oxygen-ion-conducting electrolyte (e.g., yttria-stabilized zirconia [YSZ] or scandia-stabilized zirconia [ScSZ]) is generally used in SOECs [14]. For electrically conducting electrodes, a nickel cermet cathode, and a perovskite anode such as strontium-doped lanthanum manganite (LSM) are typically used. The interconnect plate separates the process gas streams; it must also be electrically conducting and is usually metallic, such as a ferritic stainless steel.

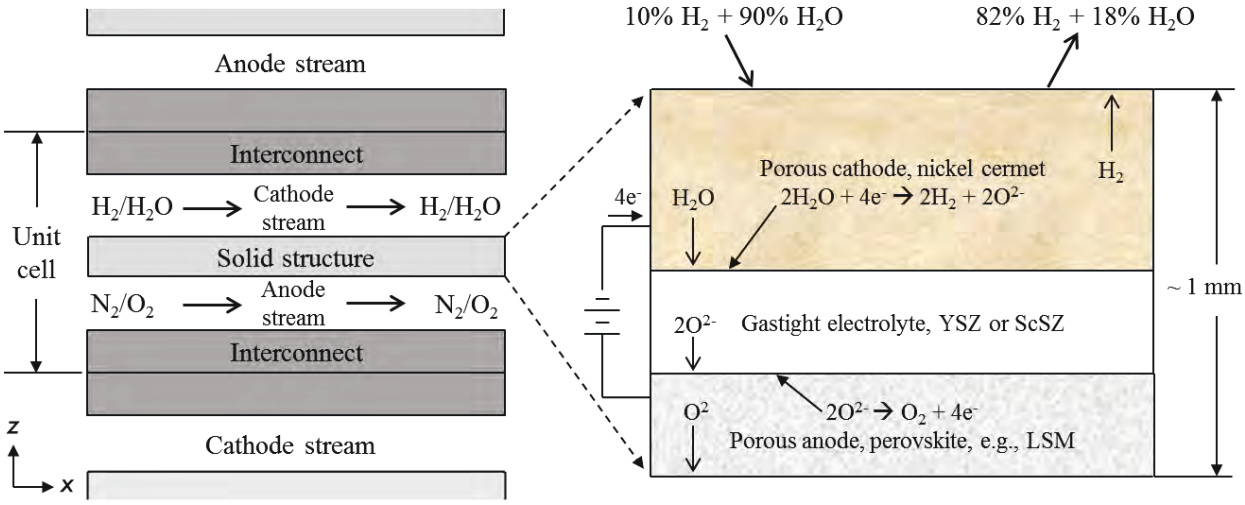

Figure 4. Cross-section of a cathode-supported planar SOEC stack. The case of co-flow is depicted.

As shown in Figure 4, a mixture of hydrogen and steam at 850°C is supplied to the cathode side of the solid structure where it is reduced into hydrogen, releasing oxide ions in the process. The half-cell electrochemical reactions take place at the triple-phase boundaries where the electrolyte, porous electrode, and gas species meet at the interfaces between the electrolyte and the electrodes [13, 14]. The oxide ions then migrate through the electrolyte (by an applied electrochemical potential) to the anode side where they recombine to form oxygen molecules, releasing electrons. An addition of 10 mole% H_2 is sufficient to avoid the oxidation of the materials (nickel cermet electrode) at an elevated temperature [15]. The outlet composition of the hydrogen-steam mixture is set to be 82 mole% H_2/18 mole% H_2O, which corresponds to the steam utilization (SU) factor, i.e., the percentage of the total inlet stream flow rate that is consumed by the electrolysis reaction, of 80%. In fact, a higher SU factor corresponds to a higher H_2 production (i.e., higher electrolysis efficiency[5]). However, it is not desirable to run the electrolyzer to 100% because localized steam starvation will occur, thus severely degrading performance [14]. The product stream exits from the SOEC stacks at 750°C, featuring an endothermic stack operation. The rationale for employing the stack in an endothermic operation is for stack temperature control with convective heating through the use of a sweep gas, which is further described in Section 2.2 in greater detail. Residual steam is removed from the outlet cathode stream by condensation. A portion of the purified H_2 is recycled to meet the desired hydrogen-steam mixture inlet composition (10 mole% H_2/90 mole% H_2O) in the cathode stream.

[5] Electrolysis efficiency quantifies the heating value of the hydrogen produced by electrolysis per unit of electrical energy consumed in the SOEC stack [14].

On the anode side of the cells, air is used as a sweep gas. Although this would remove the possibility of generating extra revenues through the sale of pure O_2, in addition to controlling the stack temperature, there are several good reasons to consider the use of a sweep gas on the anode side [14, 16]:

- Minimizes the performance degradation associated with any small leakage of hydrogen from the cathode side to the anode side of the cell.
- Alleviates serious materials issues associated with the handling of pure O_2 at elevated temperatures.
- Reduces the average mole fraction and partial pressure of oxygen, thereby reducing the open-cell and operating potentials, resulting in higher electrolysis efficiencies.

The outlet anode stream is an oxygen-enriched air (about 30 mole% O_2) and exits from the SOEC stacks at 750°C.

A dynamic high-temperature SOEC model, which consists of an electrochemical model, four mass balances, and four energy balances, was developed based on the work shown in [13, 14, 16]. The main assumptions made for the model derivation are as follows:

- In practice, an SOEC system consists of several repeating cells assembled in stacks to ensure a sufficient rate of H_2 production. However, the models of such stacks are usually constructed for the smallest unit cell (see Figure 4), which is assumed to describe the response of the whole stack subject to the use of adequate boundary conditions. In this work, the modeled unit cell is considered to be in the center of a large stack such that there are no end effects [13].
- The pressure drop along the gas channels is negligible (i.e., the cathode and anode stream velocities are assumed constant).
- The entire enthalpy change of the electrochemical reaction is assumed to occur in the solid structure. In other words, the solid structure temperature is applied in the open-cell (or Nernst) equation.
- Ideal gas behavior is assumed for the cathode and anode streams.
- The inlet air composition is 21 mole% O_2/79 mole% N_2.
- Temperatures, pressures, and compositions of the gas streams vary linearly in the axial (*x*-axis in Figure 4) direction; space-dependent effects on those operating variables are averaged by arithmetic mean.
- The convective heat transfer coefficients between the gas channels and the solid parts are assumed to be constant, given the laminar flow conditions for which the Nusselt number is considered independent of Reynolds number [17].
- The constant electrical potential is assumed along the cell as the electrodes are assumed to be good electric conductors, and, thus, it is not a local quantity.
- The properties of solid structure and interconnect (i.e., emissivity, thermal conductivity, density, and heat capacity) are constant along the cell.

Table 1 summarizes the model input parameters, such as stack geometry and material properties, and nominal operating conditions for the SOEC.

Table 1. Model input parameters and nominal operating conditions for the SOEC.

Description	Unit	Value
Cathode channel height	m	0.001
Anode channel height	m	0.001
Solid structure thickness	m	570×10^{-6}
Interconnect thickness	m	500×10^{-6}
Cell length	m	0.15
Cell width	m	0.15
Active cell area	m^2	225×10^{-4}
Cathode thickness	m	500×10^{-6}
Electrolyte thickness	m	20×10^{-6}
Anode thickness	m	50×10^{-6}
Cathode electric conductivity	Ω^{-1} m^{-1}	80×10^{3}
Anode electric conductivity	Ω^{-1} m^{-1}	8.4×10^{3}
Solid structure emissivity	–	0.8
Interconnect emissivity	–	0.1
Solid structure density	kg m^{-3}	5900
Interconnect density	kg m^{-3}	8000
Solid structure heat capacity	J kg^{-1} K^{-1}	500
Interconnect structure heat capacity	J kg^{-1} K^{-1}	500
Solid structure thermal conductivity	W m^{-1} K^{-1}	2
Interconnect thermal conductivity	W m^{-1} K^{-1}	25
Cathode stream thermal conductivity	W m^{-1} K^{-1}	0.194
Anode stream thermal conductivity	W m^{-1} K^{-1}	0.069
Cathode stream Nusselt number	–	3.09
Anode stream Nusselt number	–	3.09
Cathode stream inlet temperature	°C	850
Anode stream inlet temperature	°C	850
Cathode stream inlet composition	mole%	10 H_2 / 90 H_2O
Anode stream inlet composition	mole%	21 O_2 / 79 N_2
SU factor	%	80
Cell operating pressure	MPa	1.964
Average current density	A cm^{-2}	0.5
Average operating voltage per cell	V	1.185

As shown in Figure 1, the steam produced by the LWR is apportioned between the balance of plant and the HTSE plant. The steam conditions are typical of LWR technology with a temperature of 318°C and a pressure of 5.8 MPa. This steam (also referred to as "nuclear process heat") is split into two streams (see Figure 2) and delivers the process heat (via the counter-flow energy recovery HXs) necessary (1) to boil, flash, and superheat the HTSE feed water (cathode stream) and (2) to heat an air flow (anode stream). These hot utility streams are merged together and sent back to the nuclear reactor after being condensed into water. After recuperation the outlet temperatures of the cathode and anode streams are 283.4°C and 259°C, respectively. The superheated HTSE feed water is then mixed with a portion of the

recycled H_2 product in order to maintain reducing conditions at the cathode prior to entering the SOEC stacks (see Figure B.3). The waste heat from the hot product streams exiting the electolyzer is recovered via the H_2/steam and sweep gas heat recuperators (see Figure 2) and is used to further amplify the temperatures of the cathode and anode streams, thus reducing the overall heat load in the HTSE process. The HTSE process requires both the cathode and anode streams to be heated to 850°C, which necessitates additional topping heat from an auxiliary heat source. This heat source could come from a combustor, electric heating, or waste heat from a neighboring process. In this assessment, it is assumed that topping heat is provided by electric heating. An electric load for the ETHs is always fulfilled first by a portion of total electricity that is directed to the HTSE plant; the remainder is directed to the SOEC stacks for electrolysis. The switchyard (see Figure 3) contains the necessary logic to appropriately apportion the total power between the ETHs and the electrolyzer.

The HTSE vessels are comprised of the H_2/steam and sweep gas HXs, ETHs, and SOEC stacks, enclosed in the green dotted box shown in Figures 2 and 3. The size of the HTSE vessel was determined based on a recent detailed commercial design and operations report by Dominion Engineering [18] and is summarized in Table 2.

Table 2. Model input parameters for the HTSE vessels.

Description	Unit	Value
Number of cells per stack	cells/stack	854
Number of stacks per module	stacks/module	4
Number of modules per level (number of columns)	modules/level	4
Number of levels per vessel	levels/vessel	5
Number of on-line vessels	vessels/system	5

Figure 5 summarizes the inputs and product streams for the LWR/HTSE integration case at the nominal operating condition. The HTSE process uses a 51.1 MW_e electrical load input, of which 5.61 MW_e is used in the ETHs, from the nuclear reactor and produces no carbon dioxide (CO_2), as summarized in Table 3. A thermal energy of 18.5 MW_{th} from the nuclear reactor is used to convert the feed water to low-temperature steam and heat the sweep gas (air), which amounts to 10.3% of the total energy consumption in the HTSE plant. The combined electrical power and heat directed to the HTSE plant from an N-R HES is about 179 MW_{th} (or 57 MW_e), applying a fixed thermal-to-electrical conversion efficiency of 31.8%. The nominal value of the cathode stream flow (4.48 kg s^{-1}) is selected to achieve the SU factor of 80%, given that a cathode stream H_2 mole fraction at the SOEC stack inlet is 0.1. The nominal value of the anode stream flow rate (23.3 kg s^{-1}) is selected to achieve the cathode stream outlet temperature of 750°C, creating the temperature difference of 100°C between the inlet and outlet in the SOEC stack. The temperature gradient of this scale is expected to result in a significant convective heat transfer between the cell components and air flow. This system at nominal operating condition can produce 0.401 kg s^{-1} (12.7 metric ton yr^{-1}) hydrogen. If steam is used as a sweep gas instead of air supplied to the anode side of the SOEC, the "assumed" oxygen production rate corresponds to 3.19 kg s^{-1} (100 metric ton yr^{-1}).

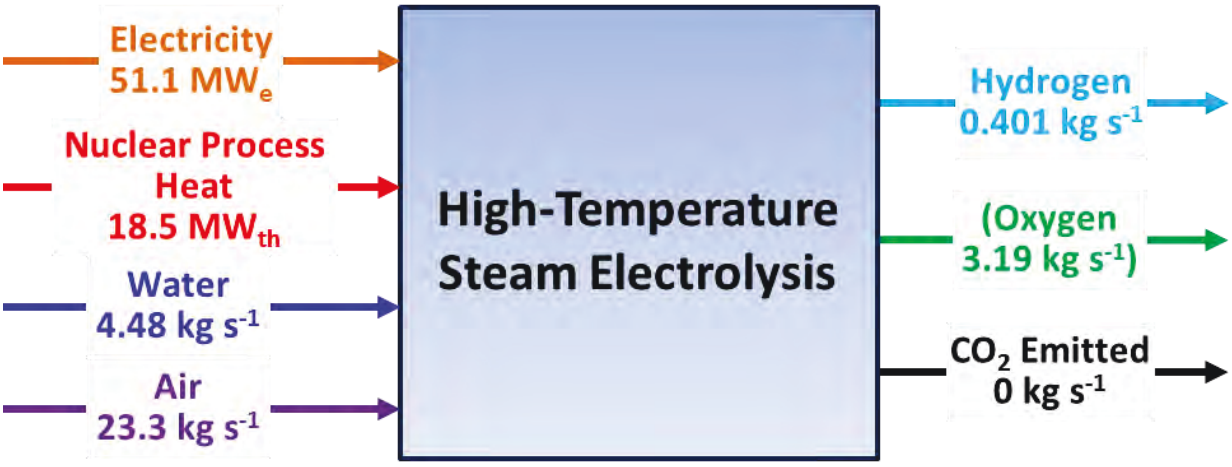

Figure 5. General energy and product flows for the LWR/HTSE integration case. The oxygen production rate is reported in parenthesis as it could "possibly" be recovered from the outlet anode stream by condensation if steam is used as a sweep gas instead of air.

Table 3. Hydrogen production summary.

	Description		Unit	Value
Inputs	Water		kg s^{-1} [metric ton yr^{-1}]	4.48 [141]
	Air		kg s^{-1} [metric ton yr^{-1}]	23.3 [734]
Outputs	Hydrogen		kg s^{-1} [metric ton yr^{-1}]	0.401 [12.7]
	(Oxygen)		kg s^{-1} [metric ton yr^{-1}]	3.19 [100]
	CO_2		kg s^{-1} [metric ton yr^{-1}]	0 [0]
Utilities	Power	Total	MW_e [MW_{th}]	51.1 [160.7[a]]
		Electrolyzer	MW_e [MW_{th}]	45.5 [143.1[a]]
		ETHs	MW_e [MW_{th}]	5.6 [17.6[a]]
	Nuclear process heat		MW_{th} [MW_e]	18.5 [5.9[b]]

[a] The thermal equivalent of the electrical power with thermal efficiency of 31.8%.
[b] The rate of heat flow expressed in terms of the electrical power equivalent with thermal efficiency of 31.8%.

2.2 Control System

Numerous feedback/feedforward controllers are augmented as low-level (regulatory) controllers to maintain the desired process conditions, such as temperatures, mass flow rates, and mole fractions at various locations in the considered HTSE plant. For the classical feedback control scheme implemented in this report, control actions (values) are calculated by PI controllers in all cases. As seen in Figure 2, the temperatures of the cathode and anode streams exiting the nuclear-heat-recuperated HXs are controlled by adjusting the openings of the two pneumatic TCVs. The temperatures of the cathode and anode streams at the SEOC stack inlets are controlled by adjusting the electrical current flowing in the ETHs (see Figure B.2).

In order to maintain the desired cathode stream H_2 mole fraction at the SOEC stack inlet, the inlet composition of the hydrogen-steam mixture needs to be either directly measured with chemical composition analyzers (such as a gas chromatograph) or indirectly estimated as a function of other process variables (such as temperature, pressure, and flow rate) that can be measured on a nearly

continuous basis. The gas chromatograph is the most commonly used on-line composition analyzer; however, a transport delay associated with the sampling, and a slow processing and analytical cycle time (updated every 3 to 10 minutes [19]) may result in an unsatisfactory control performance, i.e., an unstable oscillatory behavior in the feedback control loop. To overcome such difficulties in obtaining an on-line composition measurement with fast sampling times, the feedforward controller is developed based on the steady-state mass balance for hydrogen around the H_2/steam mixer (see Figure B.3), which relates the H_2 mole fraction of the mixture to the mass flow rates of the recycled H_2 and the pure steam. As the desired value for the H_2 mole fraction in the mixture is known, the desired H_2 mass flow to be recycled can be calculated as a function of the measured upstream steam flow rate. The output signal from the feedforward controller then serves as a set point to the PI controller for the steam flow rate. The advantage of this cascade control scheme is that it is less sensitive to control valve sticking and upstream pressure fluctuations.

Although SOEC systems are often considered for large-scale steady-state operation [16], stack temperature control becomes critical if the systems are to be used in dynamic operation, acting as FLRs, with a variable electrical load (VEL) input requested to the HTSE plant. To prevent the fracture of delicate SOEC stack components during dynamic operation, significant thermal excursions in the stack should to be avoided by the implementation of an effective control strategy. Previous work has indicated that the maximum allowable total temperature difference along a 0.1 m cell is 100°C [20], otherwise the cell is at the risk of breakdown. One possible solution to achieving the temperature control requirement is to operate the stack in an endothermic operating mode – in which the heat generated by via irreversible losses (i.e., ohmic losses, activation and concentration overpotentials) is smaller than the thermal energy consumed by the electrolysis reaction, resulting in a decrease in the temperature as the reaction proceeds along the stack [16]. Such an operation mode can facilitate the convective heat transfer between the cell components and a heated sweep gas (air), providing heating to endothermic stacks. Thus, the cathode stream temperature at the SOEC stack outlet is controlled by regulating the air flow rate on the anode side, enabling temperature control of the stack (see Figure B.1). Note that a thermoneutral operating mode, in which the thermal energy consumed by the reaction is precisely matched by the heat generated via irreversible losses, simplifies thermal management of the stack since no significant excess gas flow is required and component thermal stresses are minimized [14]. However, only a small dependence of the temperature on the air flow has been observed for a stack driven at conditions near thermoneutral operation, indicating, in general, that this operating mode should be avoided from a control perspective [21].

During dynamic operation of SOEC stacks, an SU factor changes as a function of the VEL directed to the SOEC stacks unless the cathode stream flow rate is regulated accordingly. From the stack efficiency point of view, a low SU factor is preferred. It is also important for the SU factor to be low enough to avoid a significant increase in the cathode concentration overpotential caused by steam starvation near the cell outlet [13, 15]. However, a reduction in the SU factor would result in an increased cathode stream flow rate for a given H_2 production rate, leading to increased operations and maintenance costs involved in accommodating the increased flow rate. Consequently, the SU factor should be adequately maintained near its design value under variable operating conditions. This is accomplished by adjusting the feedwater flow rate, thereby regulating the cathode stream flow rate at the SEOC stack inlet. As in the case of the H_2 mole fraction control, the SU factor control also utilizes a cascade control scheme (see Figure B.1). In this case, the feedforward controller is developed based on the steady-state mass balance for stream around the SOEC stacks, which relates the cathode stream inlet flow rate to the cathode stream outlet flow rate, SU factor, and inlet H_2 mole fraction. As the desired value for the inlet H_2 mole fraction in the mixture and that for the SU factor are known, the desired cathode stream inlet flow rate can be calculated as a function of the measured cathode stream outlet flow rate. The output signal from the feedforward controller then serves as a set point to the PI controller for the cathode stream flow rate. Table 4 summarizes the controllers (single-input single-output scheme), with their set-point values, used in the proposed HTSE system.

Table 4. Regulatory controllers used in the HTSE plant.

Functionality	Controller type	Controlled variable	Set-point value
Regulate cathode stream temperature	Feedback (PI)	Cathode stream temperature at the cathode HX outlet	283.4°C
Regulate anode stream temperature	Feedback (PI)	Anode stream temperature at the anode HX outlet	259°C
Regulate cathode stream composition	Cascade (feedforward/ feedback [PI])	Cathode stream H_2 mole fraction at the SOEC stack inlet	0.1
Regulate cathode stream temperature	Feedback (PI)	Cathode stream temperature at the SOEC stack inlet	850°C
Regulate anode stream temperature	Feedback (PI)	Anode stream temperature at the SOEC stack inlet	850°C
Regulate SOEC stack temperature	Feedback (PI)	Cathode stream temperature at the SOEC stack outlet	750°C
Regulate steam consumption during electrolysis	Cascade (feedforward/ feedback [PI])	SU factor	80%

2.3 Case Studies

Three case studies (Cases 1–3) are conducted to analyze the dynamic performance of the LWR/HTSE integration case. The key process variables (controlled variables listed in Table 4 and their corresponding MVs, as well as hydrogen and oxygen production rates) are observed to evaluate the technical feasibility and safety of such a system operating under highly flexible conditions. Key assumptions employed for the case studies performed are as follows:

- A power-smoothing battery is used to smooth the high variability introduced by either PV or wind energy, acting as a low-pass filter. The power-smoothing effect of such an electric battery is modeled as a first-order differential equation with a time constant of 1800 s (30 min).
- Renewable energy generation is modeled as a time-series input signal to the power-smoothing battery based on solar irradiance and ambient temperature data for a PV system or based on wind speed data for a wind farm [1, 2]. Historical data of solar irradiance and ambient temperature at Southwest Solar Research Park in Phoenix, Arizona[6] and that of wind speed measured in West Texas[7] were obtained from the National Renewable Energy Laboratory database and used in the case studies. For the mathematical models and the values of model parameters used to calculate PV solar and wind powers in this report, see References [2, 3].
- At typical SOEC stack temperatures and irreversible losses values, operation at the thermoneutral voltage yields current densities in the 0.2–0.6 A cm^{-2} range, which is very close to the current density range that has yielded successful long-term operation in SOFC stacks [14]. For this

[6] Accessed on October 5, 2016 at http://www.nrel.gov/midc/ssrp/

[7] Accessed on October 5, 2016 at http://www.nrel.gov/grid/wind-integration-data.html

reason, the minimum turndown of the HTSE plant (21 MW_e, of which 16.6 MW_e is delivered to the SOEC stacks) is selected to correspond to the lower bound of the considered current density range. This ensures that the plant is operated continuously with a minimum load, even when no renewable power is provided to the system. Thus, within N-R HESs, it is assumed that a minimum load of 21 MW_e is always distributed to the HTSE process.

- Pre-compressed feed streams (feed water and air) are assumed to be available at 2.143 MPa; thus the HTSE vessels are the only units that consume the electricity in the HTSE plant.

Table 5 lists the simulation setup values used in each case scenario considered.

Table 5. Simulation setup values used in the case studies for the LWR/HTSE integration.

Case No.	Renewable energy		VEL delivered to HTSE process, $L_{E,\ HTSE}$ (MW_e)	Simulation output interval, Δt (s)
	Type	Generation (MW_e)		
1	N/A	0	51.1 to 41 (step change)	1
2	PV solar	0–30	21–51 (variable)	60
3	Wind	0–28.8	21–49.8 (variable)	60

2.3.1 Case 1: Plant responses during a step change imposed on the VEL

A step change in the VEL directed to the HTSE plant ($L_{E,\ HTSE}$) has been imposed, replicating the situation in which changes in the supply of input electrical power are experienced or the sudden switch-off of the stack. Initially, the system has settled to its nominal operating condition. The transient was initiated at 1.67 min (100 s) via a 10.1 MW_e step decrease in the $L_{E,\ HTSE}$ from an initial load level of 51.1 MW_e (Figure 6(a)). The total power was subsequently apportioned (via the switchyard) between the electrolyzer ($P_{e,\ SOEC}$ in Figure 6(a)) and the ETHs ($P_{e,\ ETH}$ in Figure 6(b)). It can be seen from Figure 6(b) as the $L_{E,\ HTSE}$ decreased, so did the thermal energy consumed for heat recuperation in the HXs ($P_{e,\ HX}$); however, decreased $L_{E,\ HTSE}$ resulted in an increase in the $P_{e,\ ETH}$. Detailed discussion for this behavior is provided with figures later in this section. As can be seen, both the hydrogen (Figure 6(c)) and oxygen (Figure 6(d)) production rates are proportional to the load, i.e., an average current density is directly proportional to the electrolysis reaction rate.

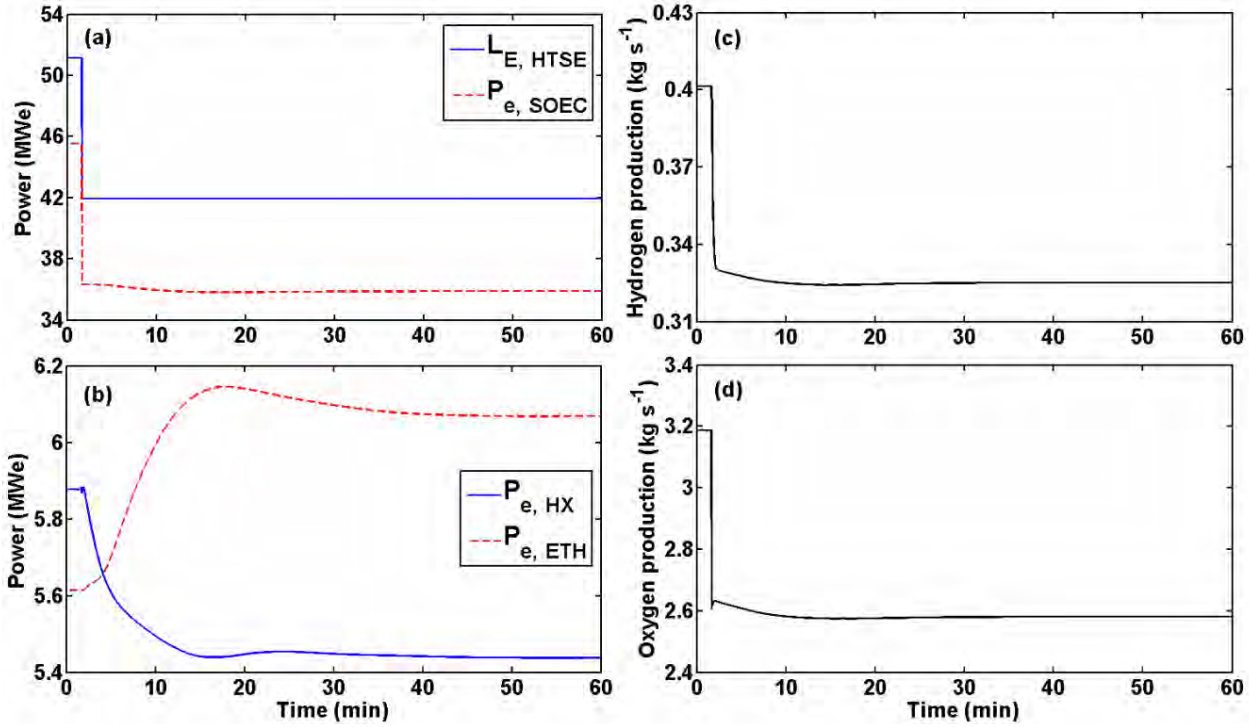

Figure 6. Case 1 results: (a) VEL directed to the HTSE plant ($L_{E,\ HTSE}$) and electrical power consumption in the SOEC stacks ($P_{e,\ SOEC}$), (b) rate of process heat flow expressed in terms of the electrical power equivalent across the HXs ($P_{e,\ HX}$) and electrical power consumption in the ETHs ($P_{e,\ ETH}$), (c) hydrogen production rate, and (d) oxygen production rate.

Figure 7 shows the responses of the controlled variables (CVs) and manipulated variables (MVs) associated with the electrolyzer following the step change made in the electric load. The instantaneous fall of the SU factor visible in Figure 7(a) is attributed to the immediate fall in the reaction rate, resulting in less consumption of the steam during electrolysis. The cathode stream flow was decreased accordingly (Figure 7(b)), gradually increasing the SU factor back to its desired value within about 25 min. Note that this control strategy would result in a decreased utility consumption involved in heating the decreased cathode flow prior to entering the SOEC stacks. In Figure 7(c), a rapid fall in the cathode stream temperature at the SOEC stack outlet is observed immediately after the negative step change in the input load imposed. This is attributed to a decrease in the heat generated via irreversible losses, following the step decrease, which was not sufficient to provide the entire thermal energy consumed by the reaction. Consequently, the temperature decreased as the reaction proceeded along the cell. Subsequently, a decrease in the heat generated via irreversible losses was offset by the increased anode stream flow rate (Figure 7(d)), resulting in increased convective heating to the stack, thereby causing the stack temperature to rise back up to the set point. The outlet temperature was brought back to the set point within about 50 min after the step change. Figure 8 shows the corresponding time series for the solid structure temperature gradient. As can be seen in the figure, the temperature gradient was kept lower than the maximum allowed temperature gradient (10°C cm^{-1}), indicating that the stack was under safe operation during the simulation time. This result suggests that the proposed control strategy has a good potential to prevent the fracture of delicate stack components, which is related to the temperature fluctuations during dynamic operation of an SOEC stack.

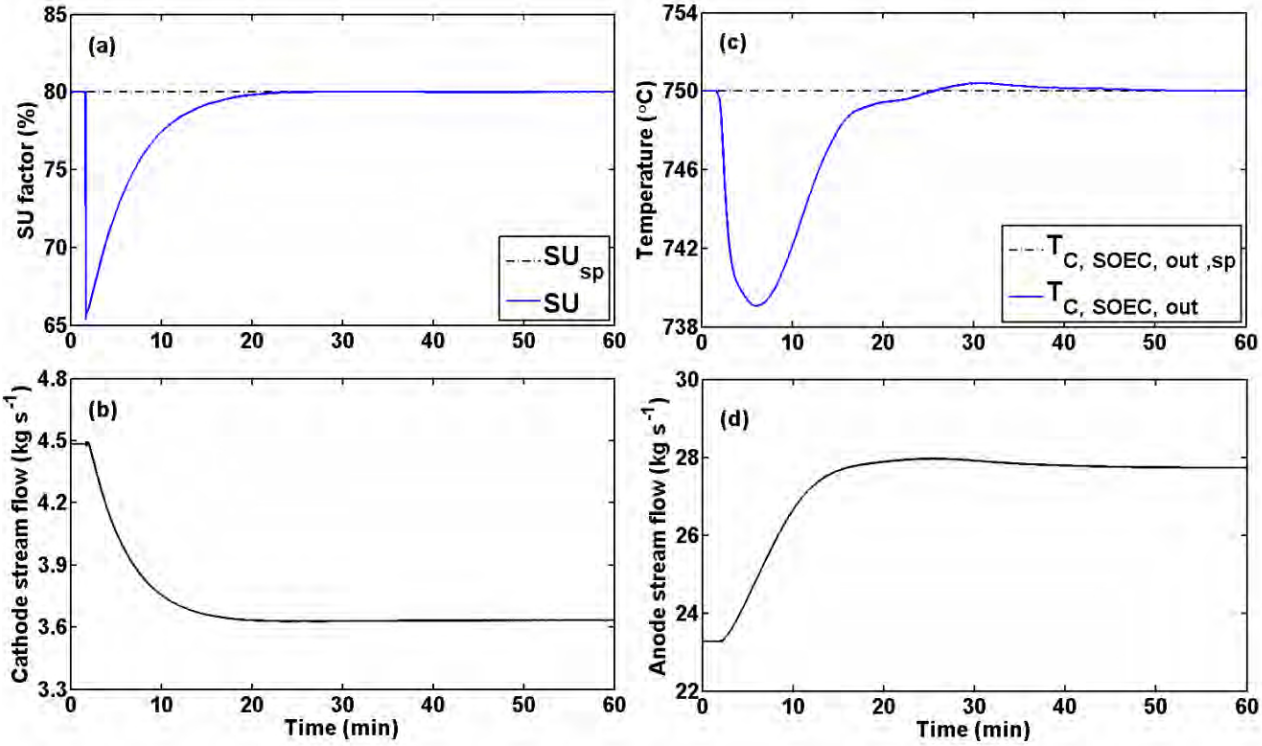

Figure 7. Case 1 results – *Electrolyzer*: (a) desired (SU_{sp}) vs. actual (SU) SU factor, (b) cathode stream (feedwater) flow rate, (c) desired ($T_{C,\,SOEC,\,out,\,sp}$) vs. measured cathode stream temperature at the SOEC stack outlet ($T_{C,\,SOEC,\,out}$), and (d) anode stream (air) flow rate.

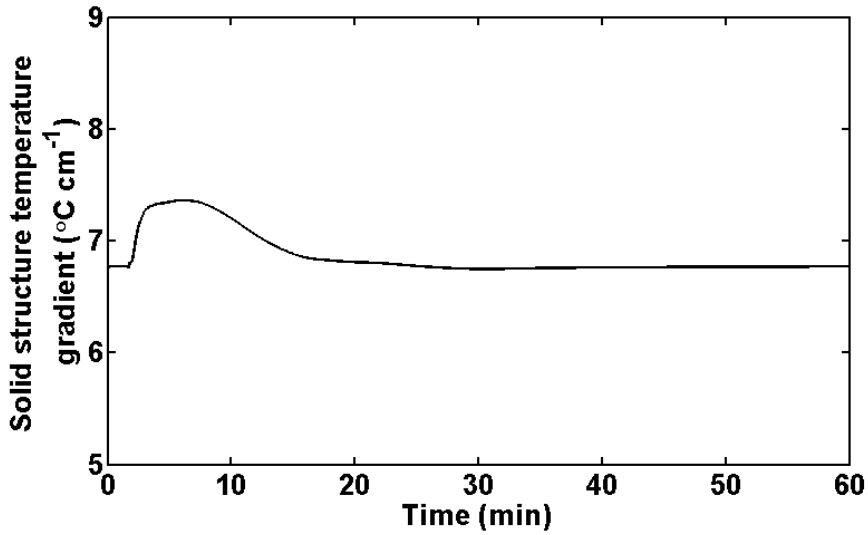

Figure 8. Case 1 result – *Electrolyzer*: solid structure temperature gradient.

Figure 9 presents the transient responses associated with the nuclear-heat-recuperated HXs following the step change made in the $L_{E,\,HTSE}$. Initially, the outlet cathode stream temperature (Figure 9(a)) increased in response to the decreased cathode stream flow rate. The TCV decreased its opening (Figure 9(c)) accordingly in order to decrease the steam flowing through the cathode HX (Figure 9(b)). This

facilitated decreased convective heat transfer between the steam drawn from the LWR and the cathode stream, and brought the temperature back to the set point within about 40 min after the step change. Conversely in Figure 9(d), the outlet anode stream temperature decreased in response to the increased anode stream flow rate. In this case, the TCV increased its opening (Figure 9(f)) in order to increase the steam flowing through the anode HX (Figure 9(e)), resulting in increased convective heat transfer between the steam drawn from the LWR and the anode stream. It required about 45 min for the anode stream temperature to match the corresponding set point and to settle to its final value.

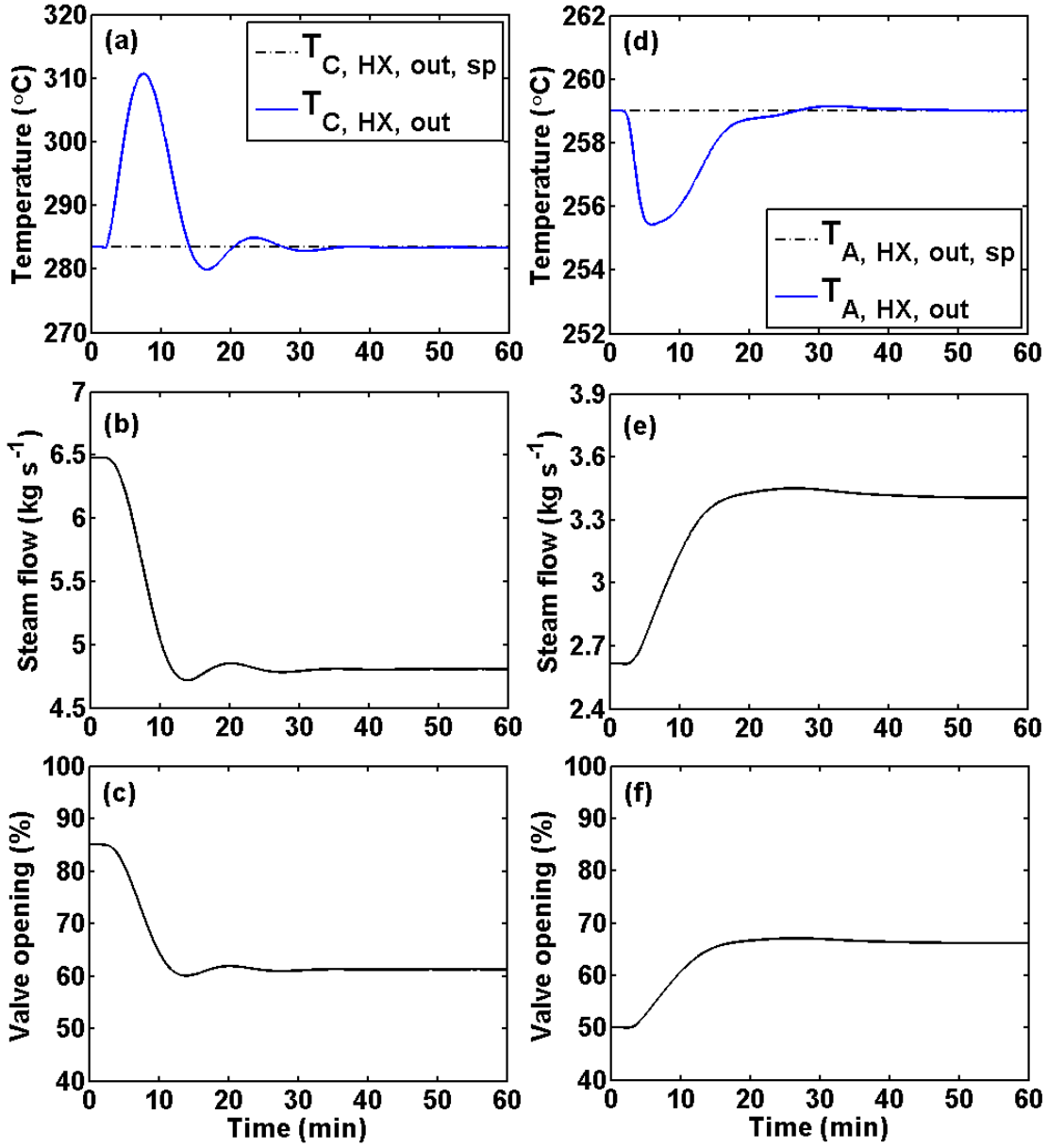

Figure 9. Case 1 results – *Nuclear-heat-recuperated HXs*: (a) desired ($T_{C, HX, out, sp}$) vs. measured ($T_{C, HX, out}$) cathode stream temperature at the cathode HX outlet, (b) cathode stream flow rate, (c) valve opening of the TCV that regulates the steam flow entering the cathode HX, (d) desired ($T_{A, HX, out, sp}$) vs. measured ($T_{C, HX, out}$) anode stream temperature at the anode HX outlet, (e) anode stream flow rate, and (f) valve opening of the TCV that regulates the steam flow entering the anode HX.

Figure 10 presents the transient responses associated with the ETHs during a step change imposed on the $L_{E,\ HTSE}$. They show essentially the same results as in Figure 9 but with a different MV, i.e. an electric current. The fall (Figure 10(c)) and rise (Figure 10(f)) in the electric current caused the cathode and anode stream temperatures to decrease (Figure 10(a)) and increase (Figure 10(d)) by consuming less (Figure 10(b)) and more (Figure 10(e)) electricity in the ETHs, respectively. The observed settling times of the controlled variables are 35 min and 20 min for the cathode and anode stream temperatures, respectively.

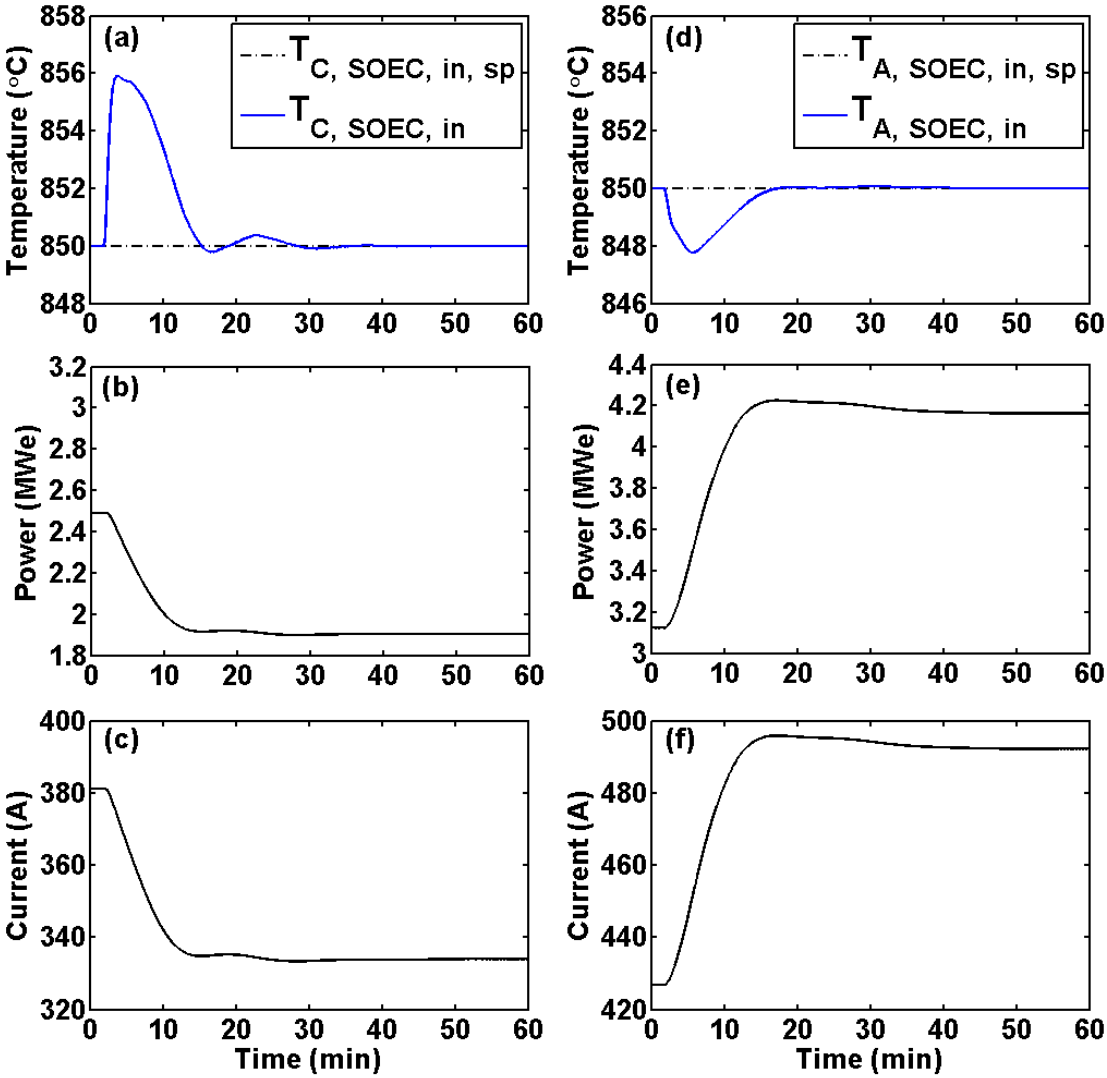

Figure 10. Case 1 results – *ETHs*: (a) desired ($T_{C,\ SOEC,\ in,\ sp}$) vs. measured ($T_{C,\ SOEC,\ in}$) cathode stream temperature at the SOEC stack inlet, (b) electric load for an ETH that heats up the cathode stream, (c) electric current for the cathode stream ETH, (d) desired ($T_{A,\ SOEC,\ in,\ sp}$) vs. measured ($T_{A,\ SOEC,\ in}$) anode stream temperature at the SOEC stack inlet, (e) electric load for an ETH that heats up the anode stream, and (f) electric current for the anode stream ETH.

Figure 11 shows the corresponding time series (transient responses) regarding the H_2/steam mixer. The rise in the cathode stream H_2 mole fraction (Figure 11(a)) is attributed to the rise in the inlet cathode stream (pure steam) flow prior to entering the mixer (Figure 11(b)). The H_2 mole fraction in the mixture settled to its set point, with a small interim excursion (an increase of 1.2%) within 25 min, by progressively reducing the amount of hydrogen recycled from the product stream (Figure 11(c)).

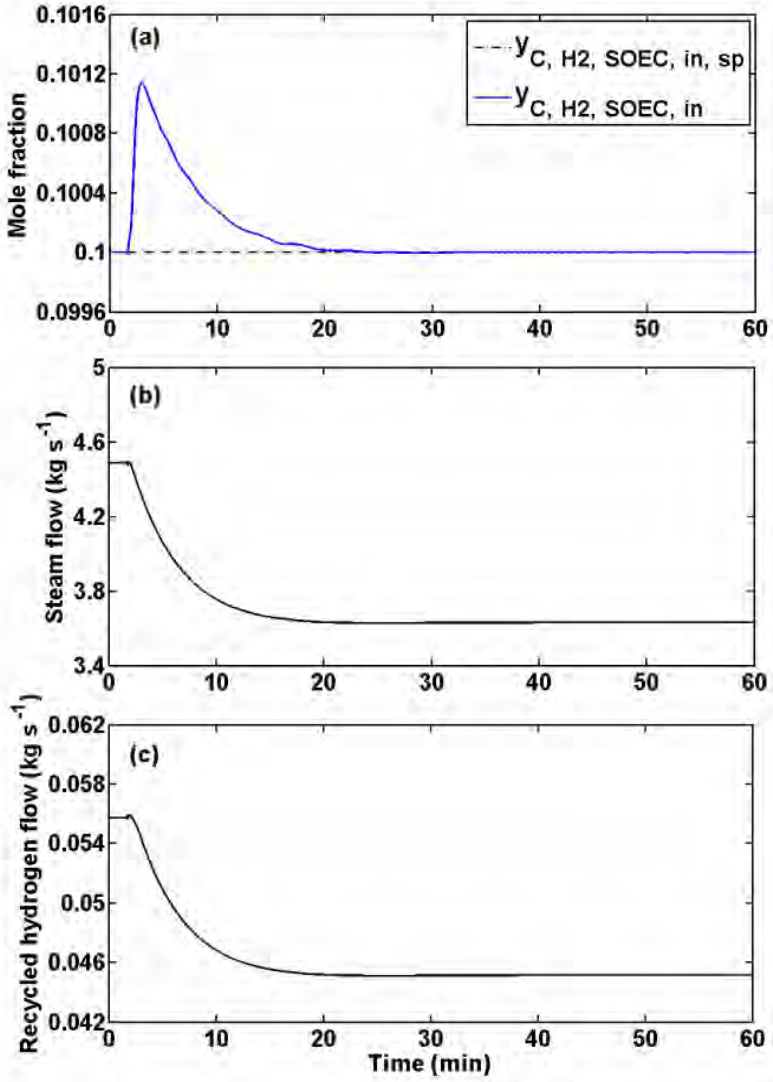

Figure 11. Case 1 results – *H_2/steam mixer*: (a) desired ($y_{C, H2, SOEC, in, sp}$) vs. measured ($y_{C, H2, SOEC, in}$) cathode stream H_2 mole fraction at the SOEC stack inlet, (b) steam flow rate, and (c) recycled hydrogen flow rate.

2.3.2 Case 2: Load-following responses with PV solar power

In Case 2, the load-following capability of the proposed HTSE plant as an FLR under variable PV solar power generation was demonstrated. Figure 12 shows the time series of a VEL (i.e., PV solar power plus a constant minimum load [21 MW_e]) delivered to the plant, hydrogen and oxygen production rates, and CVs simulated for one week. As can be seen in the figure, the plant can maintain all the CVs (Figure 12(c)–(h)) near their desired set points regardless of the time-varying electrical load delivered to the plant (Figure 12(a)), while supporting hydrogen and oxygen production (Figure 12(b)). These results suggest that the HTSE process integrated N-R HES, with a high penetration of renewable generation, has a good potential to act as a highly responsive device to meet load-following needs by accordingly delivering the necessary electricity generation profile demanded by the electric grid, while correspondingly adjusting itself to maintain adequate operating conditions. Moreover, since the HTSE plant can be operated at its minimum turndown for as long as requested, the N-R HES configuration including the HTSE plant can maintain the change in its electrical production for a long enough duration.

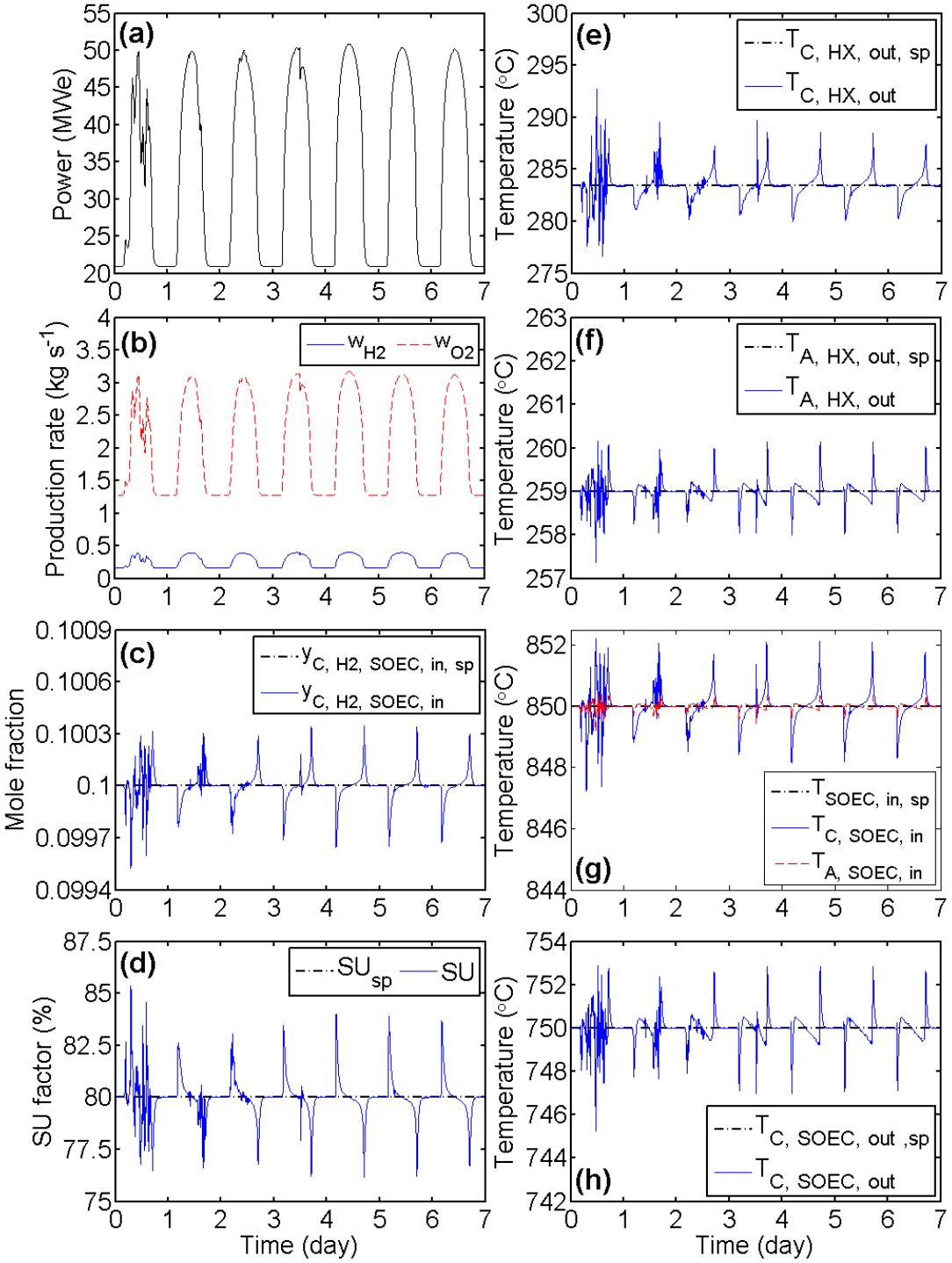

Figure 12. Case 2 results: (a) PV solar power generation, (b) hydrogen (w_{H2}) and oxygen (w_{O2}) production rates, (c) desired ($y_{C, H2, SOEC, in, sp}$) vs. measured ($y_{C, H2, SOEC, in}$) cathode stream H_2 mole fraction at the SOEC stack inlet, (d) desired (SU_{sp}) vs. actual (SU) SU factor, (e) desired ($T_{C, HX, out, sp}$) vs. measured ($T_{C, HX, out}$) cathode stream temperature at the cathode HX outlet, (f) desired ($T_{A, HX, out, sp}$) vs. measured ($T_{C, HX, out}$) anode stream temperature at the anode HX outlet, (g) desired temperature at the SOEC stack inlet ($T_{SOEC, in, sp}$) vs. measured cathode ($T_{C, SOEC, in}$) and anode ($T_{A, SOEC, in}$) stream temperatures at the SOEC stack inlet, and (h) desired ($T_{C, SOEC, out, sp}$) vs. measured cathode stream temperature at the SOEC stack outlet ($T_{C, SOEC, out}$).

2.3.3 Case 3: Load-following responses with wind power

This test was designed to assess the capability of the same system considered in Case 2 for load following, but in coordination with wind power generation. The results simulated for one week are plotted in Figure 13. Similar to the results shown in Case 2, the variability introduced by the renewable (wind) source was essentially accommodated by the use of the flexible electrical load provided by the HTSE plant. The plant could maintain all the CVs close to their set-point values at all times, exhibiting satisfactory control performance over the entire range of HTSE operating conditions.

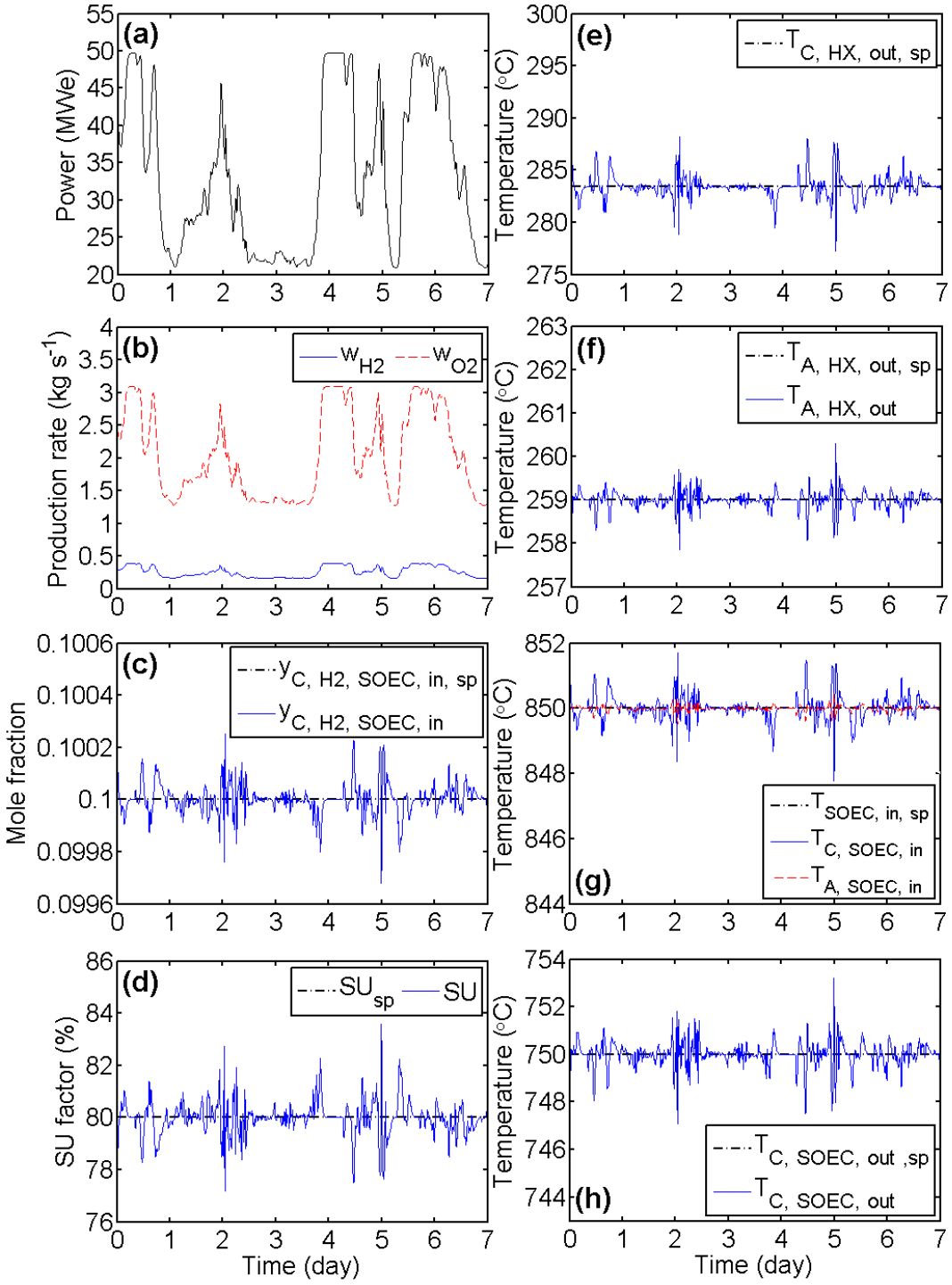

Figure 13. Case 3 results: (a) wind power generation, (b) hydrogen (w_{H2}) and oxygen (w_{O2}) production rates, (c) desired ($y_{C, H2, SOEC, in, sp}$) vs. measured ($y_{C, H2, SOEC, in}$) cathode stream H_2 mole fraction at the SOEC stack inlet, (d) desired (SU_{sp}) vs. actual (SU) SU factor, (e) desired ($T_{C, HX, out, sp}$) vs. measured ($T_{C, HX, out}$) cathode stream temperature at the cathode HX outlet, (f) desired ($T_{A, HX, out, sp}$) vs. measured ($T_{C, HX, out}$) anode stream temperature at the anode HX outlet, (g) desired temperature at the SOEC stack inlet ($T_{SOEC, in, sp}$) vs. measured cathode ($T_{C, SOEC, in}$) and anode ($T_{A, SOEC, in}$) stream temperatures at the SOEC stack inlet, and (h) desired ($T_{C, SOEC, out, sp}$) vs. measured cathode stream temperature at the SOEC stack outlet ($T_{C, SOEC, out}$).

2.4 Conclusions – High-Temperature Steam Electrolysis Plant

A dynamic performance analysis of an integration of the HTSE process with an LWR was carried out to evaluate the technical feasibility and safety of such a system operating under highly variable conditions requiring flexible output. To support the dynamic analysis, the detailed dynamic model and control design of the HTSE process, which employs SOEC stacks, have been developed to predict the process behavior over a large range of operating conditions. As an LWR would have a relatively low reactor outlet temperature, the complimentary temperature-boosting technology was suggested for integration with the HTSE process that requires higher temperature input. The case study results show that the suggested control scheme could maintain the controlled variables within desired limits under various plant operating conditions. The results also show that the proposed HTSE plant, when integrated within an N-R HES, can respond quickly and maintain the required change for a long enough duration in response to large, rapid net demand variations. The ability for HTSE to respond quickly can support renewable integration and various types of ancillary services, such as operating reserves (regulating, ramping, and load following). Its operational flexibility and the variety of potential N-R HES configurations in which it can be integrated make HTSE a good candidate for integration from a technical point of view.

3. GAS TURBINE POWER PLANT

Recently, natural gas-fired turbines have found widespread use because of their higher efficiencies; lower capital costs; shorter installation times; abundance of natural gas supplies; lower greenhouse gas emissions compared to other energy sources; and fast start-up capability, which enables them to be used as peaking units that respond to peak demands [22, 23]. Due to their special characteristics, natural gas-fired turbines are installed in numerous places around the world and have become an important source for power generation. This section is dedicated to detailed process and control designs of the GTPP, whose primary role is to cover rapid dynamics in grid demand that cannot be met by the remainder of the N-R HES. Simulation results involving several case studies are also provided.

3.1 System Overview

Figure 14 shows the top-level model for the GTPP implemented in Modelica. As seen in the figure, nine main subsystems can be identified as follows:

Physical devices:

1. Compressor
2. Combustor
3. Turbine
4. Rotational component with inertia
5. Active power generator

Control devices:

6. Classical feedback controllers (two PI controllers and two integral controllers, shown in Figure 16)
7. Low value selector (LVS)
8. Control bus

System-wide setting:

9. System component

Each of these subsystems consists of a number of basic components. Detailed descriptions of the basic components are beyond the scope of this report.

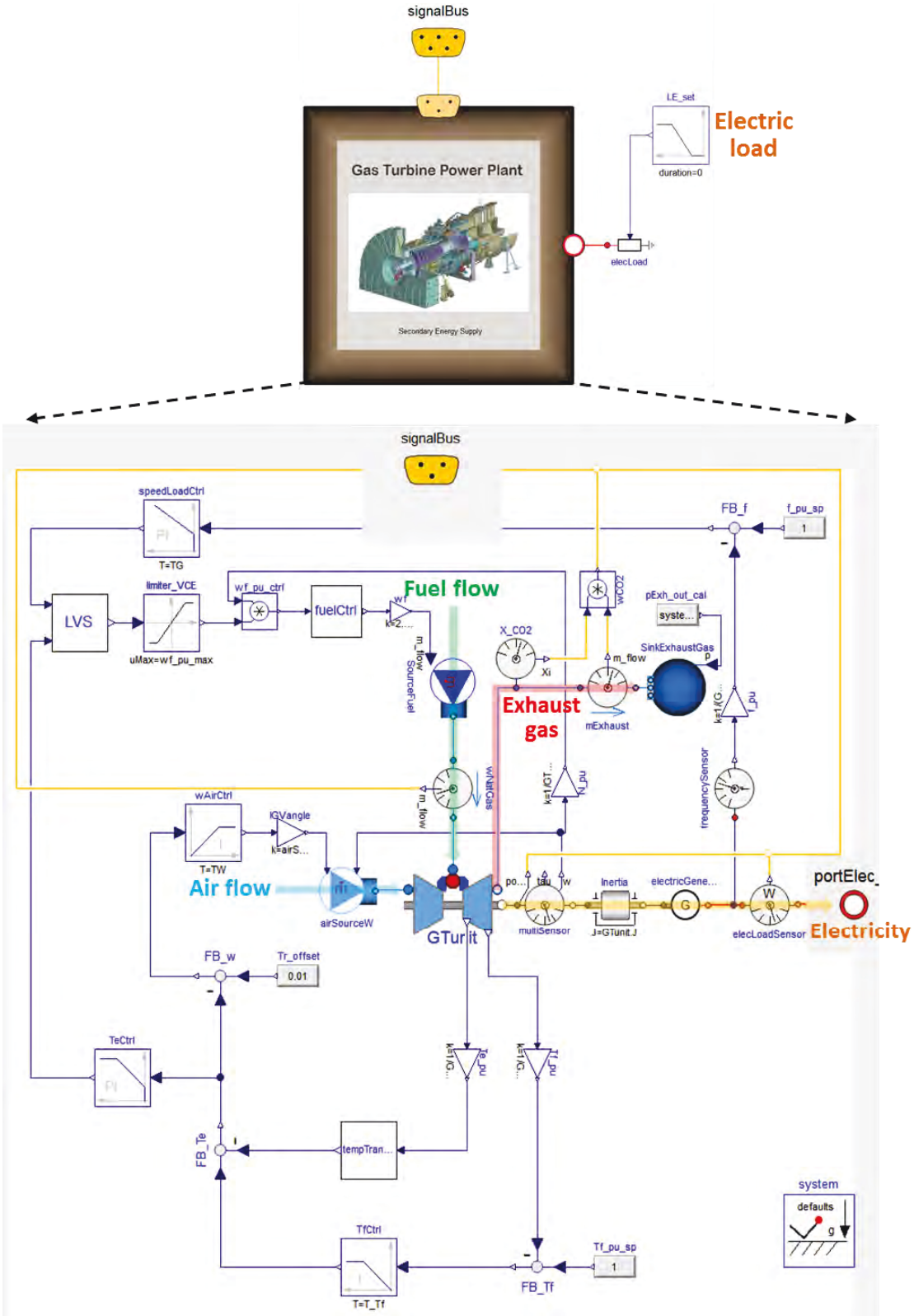

Figure 14. Top-level model for the GTPP in Modelica.

A schematic of a single-shaft heavy-duty gas turbine (HDGT) is shown in Figure 15. A gas turbine works with the Brayton cycle. As can be seen in Figure 15, air with atmospheric conditions at point 1 is compressed adiabatically by the compressor to point 2. Segment 2–3 pertains to isobaric heating of compressed air in the combustor, which increases the temperature to point 3. The combustion product and compressor discharge air at point 3 will enter the turbine and expand adiabatically to point 4. The pressure loss in the air filters and the combustion chamber is neglected [24]. The net energy supplied to HDGT is the difference between the mechanical power generated by the turbine and the power consumed by the compressor. Note that a greater difference between the turbine inlet and outlet temperatures allows more work to be extracted from the expanding gases.

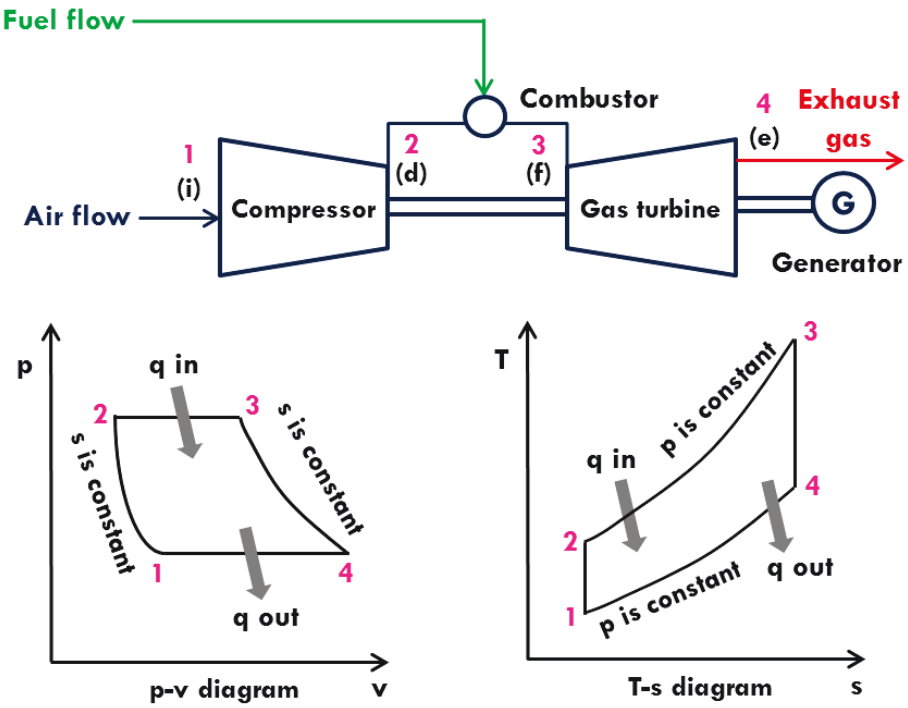

Figure 15. Schematic of a single-shaft HDGT (upper), and P-v (lower left) and T-s (lower right) diagrams of an ideal Brayton cycle (q: heat, p: pressure, v: volume, T: temperature, s: entropy).

In this report, the model used to capture the nonlinear dynamics of the GTPP is based on the work shown in [23, 25-27]. It is expected that the model is valid for variations in rotational speed of the rotor shaft from 95% to 105% and for unit loading above about 50% load [25]. In deriving the gas turbine model parameters, the efficiencies of the units (compressor, combustor, and turbine), the specific heat of the working fluids (air and exhaust gas), and the lower heating value (LHV) of the fuel (natural gas) were assumed to be constant. Also, a gas turbine shows a very fast dynamic response due to small time constants, some of which are less than 0.2 s, so a steady-state assumption is valid for the gas turbine dynamics [23, 25, 26, 28-30]. The model input parameters and nominal operating conditions are listed in Table 6.

Table 6. Nominal data of the GTPP selected for modeling.

Description	Unit	Value
Net power output	MW_e	35
Nominal frequency	Hz	60
Rotational speed of the rotor shaft	RPM	3600
Lumped rotor inertia	kg m^2	2649
Air flow rate	kg s^{-1}	108
Fuel flow rate	kg s^{-1}	2.27
Gas turbine firing temperature	°C	1067
Exhaust gas temperature	°C	514
Pressure ratio	–	13
LHV of the fuel (natural gas)	kJ kg^{-1}	43094
Turbine efficiency	%	89
Compressor efficiency	%	86
Combustion efficiency	%	99

3.2 Control System

The three main CVs in a GTPP are the rotor speed N, exhaust gas temperature T_e, and turbine firing temperature T_f. Once the generator is synchronized and connected to the power grid, the power imbalance between the generator power output P_m and electric load L_E will cause the deviation of the grid frequency unless it is controlled properly. Therefore, the rotation speed (frequency) of the rotor shaft in the gas turbine must be controlled at its nominal frequency all the time. The turbine's exhaust gas temperature needs to be kept lower than its reference temperature so as to not damage the gas turbine, yet high enough to achieve high efficiency. To regulate nitrogen oxide emissions, the turbine firing temperature also needs to be kept lower than a specified upper limit. These CVs are controlled by manipulating two variables: fuel demand, F_d, to vary the fuel flow, and compressor inlet guide vanes (IGVs) to schedule air flow. Possible disturbance variables are ambient air conditions (temperature, pressure, and relative humidity) and an electric load.

Figure 16 shows a simplified block diagram for the single-shaft HDGT proposed, together with its classical feedback control system employed in this study. Note that the variables shown in Figure 16 are normalized by their rated values at nominal operating condition and expressed in per unit values, pu (per unit values are the decimal equivalents of percent values). In the percent system, 100 equals the design value, while in the per unit system 1.00 equals the design value [28, 29].

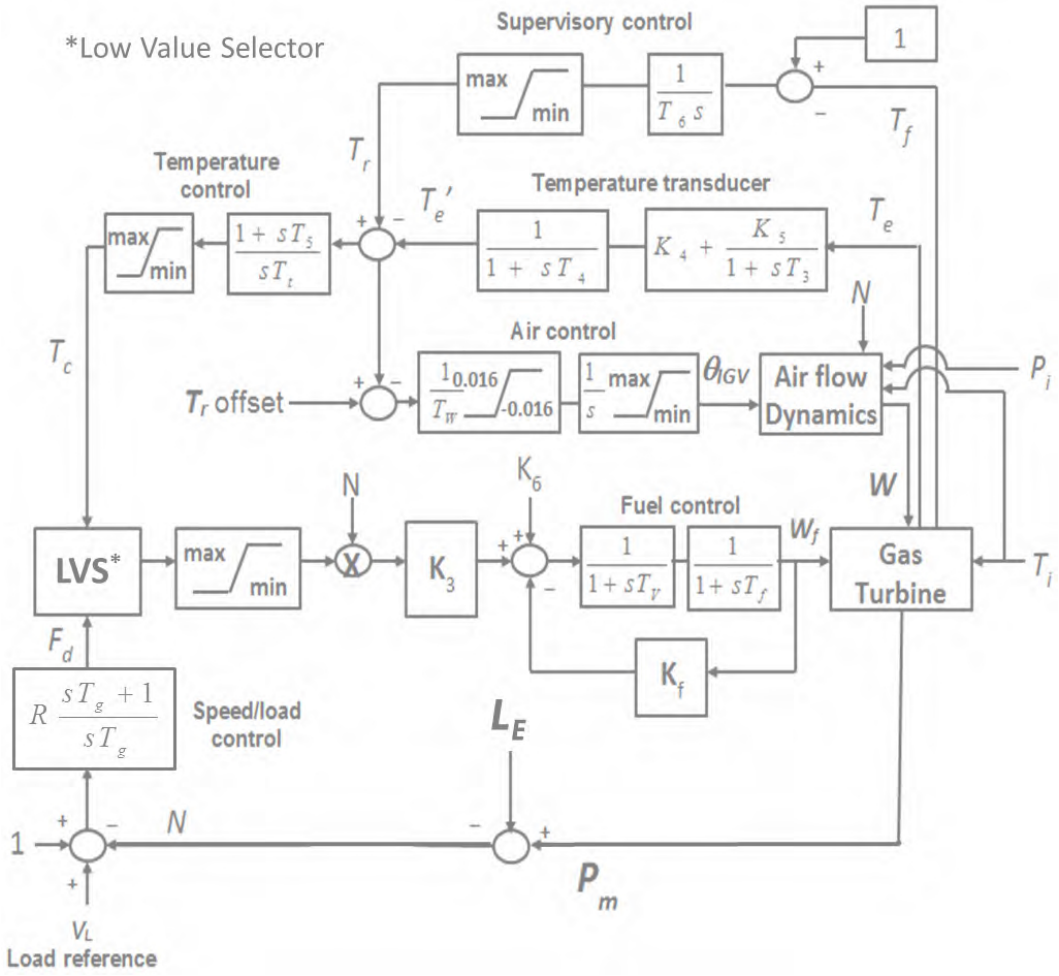

Figure 16. Simplified gas turbine simulation block diagram [23, 27].

First-order dynamic models are used to represent the pneumatic valve positioner and valve actuator in the fuel control system as well as the radiation shield and thermocouple in the exhaust gas temperature measuring system. The speed/load control block (i.e., an isochronous speed governor) determines the fuel demand F_d according to the rotor speed deviation from the rated value (1-N) and the load reference V_L. The temperature control block prevents the turbine's exhaust temperature T_e from exceeding its reference temperature T_r. The measured exhaust gas temperature T_e' is compared with the reference temperature T_r. The temperature control signal T_c is compared with the fuel demand F_d, and the lower value is selected by the LVS, which determines the fuel flow W_f into the combustor. The fuel flow is proportional to the rotor speed N. Supervisory control defines the reference temperature T_r for the exhaust gas temperature T_e. When the turbine firing temperature T_f exceeds its rated value, supervisory control reacts by decreasing T_r. The air control block regulates the air flow W so as to achieve the desired exhaust gas temperature. The exhaust gas temperature T_e is kept lower than T_r, by an offset, i.e., 1% of its rated value. The air flow is adjusted by the angular position of the IGVs θ_{IGV}. The maximum rate of change in air flow is assumed to be 1.6 % s^{-1} [31]. The model parameters shown in Figure 16 are summarized in Table 7.

Table 7. Model parameters shown in Figure 16.

Description	Symbol	Unit	Value
Ambient air pressure reference	P_{a0}	atm	1
Ambient air temperature reference	T_{a0}	°C	15
Minimum IGV angle reference	θ_{min}	degree	11.6
Maximum IGV angle reference	θ_{max}	degree	85.0
Air flow speed factor	A_0	–	0.945
Air flow speed factor	A_1	–	-7.8
Air flow speed factor	A_2	–	39
Air control lower limit	$\theta_{IGV,\ min}$	pu[a]	0.6587
Air control upper limit	$\theta_{IGV,\ max}$	pu	1
Gain of isochronous speed governor	R	pu	30
Isochronous speed governor time constant	T_g	s	1.5
Gain of radiation shield	K_4	pu	0.85
Gain of radiation shield	K_5	pu	0.15
Radiation shield time constant	T_3	s	12.2
Thermocouple time constant	T_4	s	1.7
Temperature control time constant	T_5	s	3.3
Temperature control integration rate	T_t	s pu^{-1}	0.304
Exhaust gas temperature lower limit	$T_{c,\ min}$	pu	0
Exhaust gas temperature upper limit	$T_{c,\ max}$	pu	1.1
Fuel control lower limit	$F_{d,\ min}$	pu	-0.05
Fuel control upper limit	$F_{d,\ max}$	pu	1.5
Ratio of fuel adjustment	K_3	pu	0.894
Fuel valve lower limit	K_6	pu	0.106
Valve positioner time constant	T_V	s	0.04
Fuel system external feedback constant	K_f	pu	0
Fuel system time constant	T_F	s	0.26
Time constant of T_f control	T_6	s	60
Rated exhaust gas temperature lower limit	$T_{r,\ min}$	pu	0.968
Rated exhaust gas temperature upper limit	$T_{r,\ max}$	pu	1.01
Air control time constant	T_W	s pu^{-1}	0.304
Air valve upper limit	g_{max}	pu s^{-1}	1
Air valve lower limit	g_{min}	pu s^{-1}	0.73
T_r offset	$T_{r,\ offset}$	pu	0.01

[a] per unit value

3.3 Case Studies

Two case studies (Cases 1–2) are conducted to analyze the dynamic performance of the proposed GTPP. In all cases, the key process variables (CVs defined in Section 3.2; air and fuel flow rates; net power output; and electric power frequency (or equivalently, rotational speed of the rotor shaft) are observed to assess whether the dynamic behavior of the GTPP is satisfactory under each test. In the case studies performed, ambient air temperature and pressure are assumed to be the constant international organization for standardization (ISO) conditions (i.e., 1 atm ambient pressure and 15 °C [23]). Thus, the only disturbance considered is an electric load (L_E). Table 8 lists the simulation setup values used in each case scenario considered.

Table 8. Simulation setup values used in the case studies for the GTPP.

Case No.	Electric load, L_E (MW_e)	Simulation output interval, Δt (s)
1	21 to 28 (step change)	0.1
2	19.25–35 (random variations)	0.1

3.3.1 Case 1: Plant responses during a step change imposed on the L_E

Figure 17 shows the plant responses to an instantaneous load increase (7 MW_e) introduced at five seconds for an initial operating point corresponding to 60% of nominal power output (21 MW_e). As shown in Figure 17(d), the frequency drop through the speed/load control immediately resulted in an increase in the fuel flow rate (Figure 17(e)) in order to restore the frequency (rotor speed). However, an increased fuel flow resulted in temperature increases (Figure 17(b) and (c)), which activated the temperature control. After the first post-disturbance period of 1.5 s, the power generation was reduced to avoid overheating of gas turbine blades by decreasing the fuel flow. The activation of the temperature control resulted in a decrease in both T_e and T_f, however, this limited the fuel flow and power generation as seen in Figure 17(e) and (a). Subsequently, the fuel flow (and the corresponding power generation) could be increased again because T_e and T_f dropped due to greater air flow (Figure 17(f)). During the time between 8 s and 15 s, the slow increase in P_m is thus explained. At the time of around15 s, the LVS switched to the speed/load control again, commanding the output of the gas turbine, thereby reducing its output power and frequency. Eventually, the plant was able to recover the frequency near its nominal value (with settling time of about 15 s) and bring the exhaust gas and turbine firing temperatures below their upper limits.

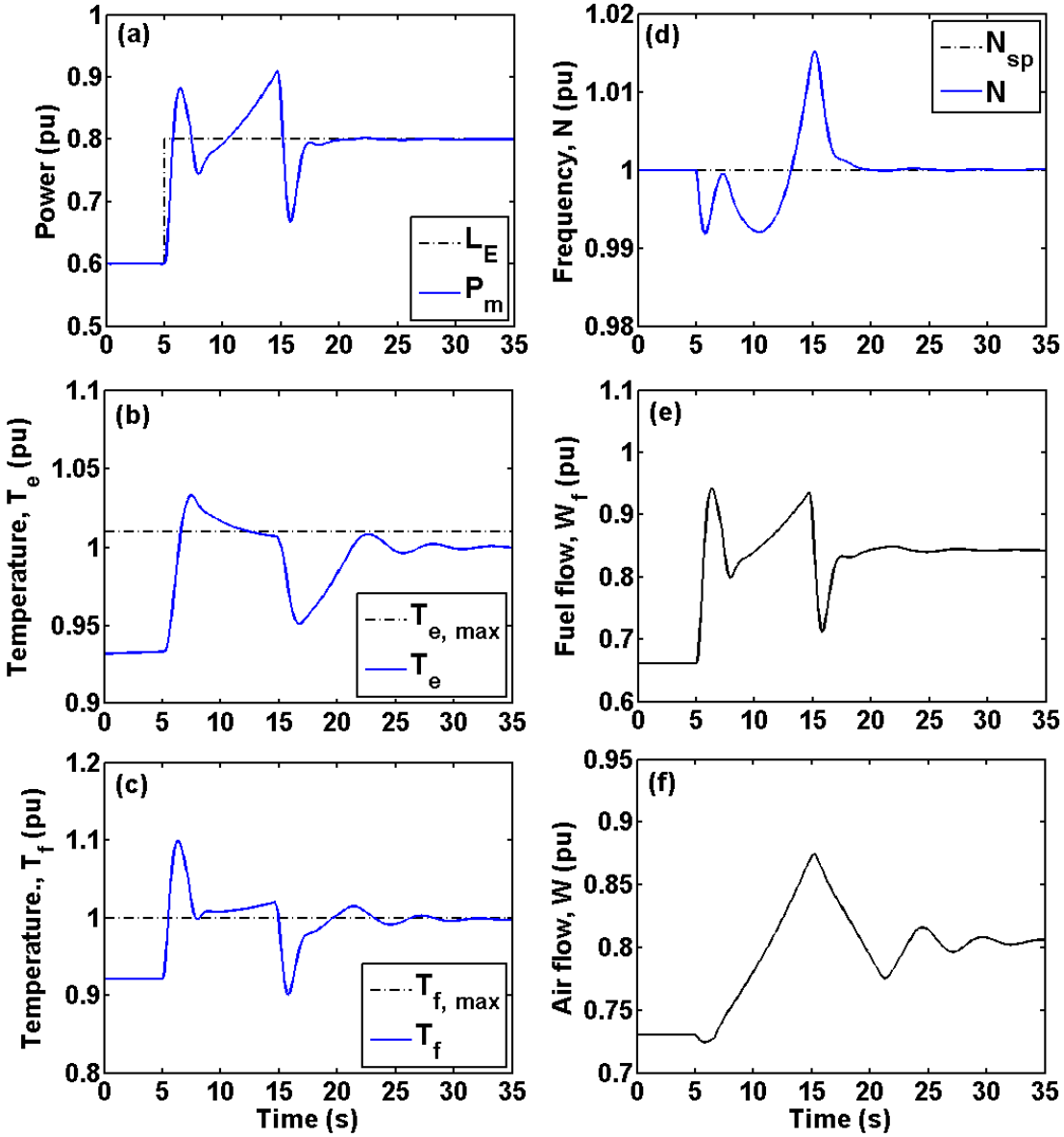

Figure 17. Case 1 results: (a) electric load (L_E) vs. power output (P_m), (b) maximum ($T_{e,\,max}$) vs. measured (T_e) exhaust gas temperature, (c) maximum ($T_{f,\,max}$) vs. measured (T_f) turbine firing temperature, (d) desired (N_{sp}) vs. measured (N) frequency, (e) fuel flow rate (W_f), and (f) air flow rate (W).

3.3.2 Case 2: Plant responses to random variations in the L_E

Figure 18 shows the output responses to random variations in the demand load simulated for one hundred seconds. The plant could maintain the frequency near its set point (Figure 18(b)) over the whole time horizon regardless of the time-varying electrical load required to match (Figure 18(a)). As observed in Figure 18(c) and (d), the temperature control scheme kept the exhaust gas and turbine firing temperatures, except for a few surges immediately after the frequency drops, below their references. These results suggest that the proposed GTPP will be able to cover rapid grid demands that the dynamics of the remainder of the N-R HES cannot handle while maintaining the high quality of electrical frequency.

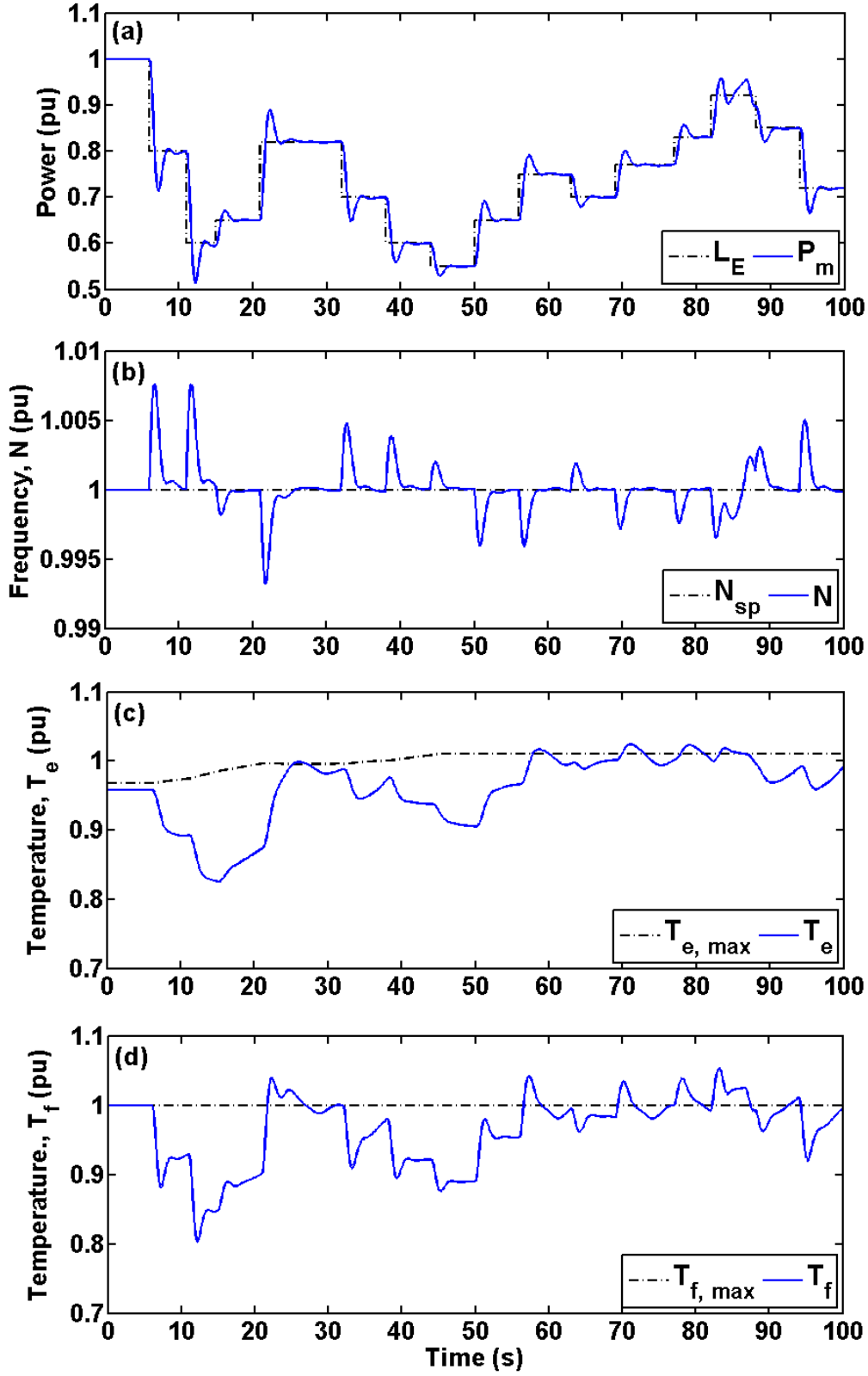

Figure 18. Case 2 results: (a) electric load (L_E) vs. power output (P_m), (b) desired (N_{sp}) vs. measured (N) frequency, (c) maximum ($T_{e,\,max}$) vs. measured (T_e) exhaust gas temperature, and (d) maximum ($T_{f,\,max}$) vs. measured (T_f) turbine firing temperature.

3.4 Conclusions – Gas Turbine Power Plant

A GTPP was proposed as an auxiliary generator to be included in an N-R HES to cover rapid dynamics in grid demand that the remainder of the system cannot follow. To predict the process behavior during transients that occur in plant operation, a dynamic simulation model was developed. To evaluate the controllability of the proposed process during dynamic operation, classical feedback controllers were implemented for power frequency and temperature controls. Several case studies were performed to investigate the system responses to the major disturbance (power load demand) in such a control system. The simulation results show that the performance of the load/frequency and temperature control systems was satisfactory under each test when the GTPP experienced high, rapid variations in the load.

REFERENCES

[1] Kim J, Garcia H. Nuclear-Renewable Hybrid Energy System for Reverse Osmosis Desalination Process. Transactions of the American Nuclear Society. 2015;112:121-4.

[2] Kim JS, Chen J, Garcia HE. Modeling, control, and dynamic performance analysis of a reverse osmosis desalination plant integrated within hybrid energy systems. Energy. 2016;112:52-66.

[3] Garcia HE, Chen J, Kim JS, McKellar MG, Deason WR, Vilim RB, et al. Nuclear Hybrid Energy Systems - Regional Studies: West Texas & Northeastern Arizona. Idaho Falls (ID): Idaho National Laboratory, Nuclear Science and Technology Division; 2015 Apr. Report No.:INL/EXT-15-34503. Contract No.:DE-AC07-05ID14517. Sponsored by the U.S. Department of Energy.

[4] Garcia HE, Chen J, Kim JS, Vilim RB, Binder WR, Bragg Sitton SM, et al. Dynamic performance analysis of two regional Nuclear Hybrid Energy Systems. Energy. 2016;107:234-58.

[5] Chen J, Garcia HE, Kim JS, Bragg-Sitton SM. Operations optimization of nuclear hybrid energy systems. Nuclear Technology. 2016;195:143-56.

[6] Fritzson P. Principles of Object-Oriented Modeling and Simulation with Modelica 3.3: A Cyber-Physical Approach: John Wiley & Sons; 2014.

[7] Rabiti C, Kinoshita RA, Kim JS, Deason W, Bragg-Sitton SM, Boardman RD, et al. Status on the Development of a Modeling and Simulation Framework for the Economic Assessment of Nuclear Hybrid Energy Systems. Idaho Falls (ID): Idaho National Laboratory, Nuclear Science and Technology Division; 2015 Sep. Report No.:INL/EXT-15-36451. Contract No.:DE-AC07-05ID14517. Sponsored by the U.S. Department of Energy.

[8] Rabiti C, Alfonsi A, Mandelli D, Cogliati J, Kinoshita R. Advanced probabilistic risk analysis using RAVEN and RELAP-7. Idaho Falls (ID): Idaho National Laboratory, Nuclear Science and Technology Division; 2014 Jun. Report No.:INL/EXT-14-32491. Contract No.:DE-AC07-05ID14517. Sponsored by the U.S. Department of Energy.

[9] Epiney AS, Kinoshita RA, Kim JS, Rabiti C, Greenwood MS. Software development infrastructure for the HYBRID modeling and simulation project. Idaho Falls (ID): Idaho National Laboratory, Nuclear Science and Technology Division; 2016 Sep. Report No.:INL/EXT-16-40004. Contract No.:DE-AC07-05ID14517. Sponsored by the U.S. Department of Energy.

[10] Bragg-Sitton SM, Boardman R, Rabiti C, Kim JS, McKellar M, Sabharwall P, et al. Nuclear-Renewable Hybrid Energy Systems: 2016 Technology Development Program Plan. Idaho Falls (ID): Idaho National Laboratory, Nuclear Science and Technology Division; 2016 Mar. Report No.:INL/EXT-16-38165. Contract No.:DE-AC07-05ID14517. Sponsored by the U.S. Department of Energy.

[11] Modelica Association. Modelica Standard Library [Internet]. [updated 2016 Apr 3; cited 2016 Sep 26]. Available: https://github.com/modelica/Modelica.

[12] Casella F, Leva A. ThermoPower [Internet]. [updated 2014 Jun 10; cited 2016 Sep 26]. Available: https://github.com/modelica-3rdparty/ThermoPower.

[13] Udagawa J, Aguiar P, Brandon NP. Hydrogen production through steam electrolysis: Model-based steady state performance of a cathode-supported intermediate temperature solid oxide electrolysis cell. Journal of Power Sources. 2007;166:127-36.

[14] O'Brien J. Thermodynamic considerations for thermal water splitting processes and high temperature electrolysis. ASME 2008 International Mechanical Engineering Congress and Exposition. Boston, Massachusetts, USA: American Society of Mechanical Engineers; 2008. p. 639-51.

[15] Cai Q, Brandon NP, Adjiman CS. Modelling the dynamic response of a solid oxide steam electrolyser to transient inputs during renewable hydrogen production. Frontiers of Energy and Power Engineering in China. 2010;4:211-22.

[16] Udagawa J, Aguiar P, Brandon NP. Hydrogen production through steam electrolysis: Model-based dynamic behaviour of a cathode-supported intermediate temperature solid oxide electrolysis cell. Journal of Power Sources. 2008;180:46-55.

[17] Palsson J, Selimovic A, Sjunnesson L. Combined solid oxide fuel cell and gas turbine systems for efficient power and heat generation. Journal of Power Sources. 2000;86:442-8.

[18] Krull P, Roll J, Varrin RD. HTSE Plant Cost Model for the INL HTSE Optimization Study. Reston (VA): Dominion Engineering, Inc.; 2013 Mar. Report No.:R-6828-00-01.

[19] Riggs JB, Karim MN. Chemical and Bio-process Control: James B. Riggs, M. Nazmul Karim: Prentice Hall; 2006.

[20] Aguiar P, Adjiman CS, Brandon NP. Anode-supported intermediate temperature direct internal reforming solid oxide fuel cell. I: model-based steady-state performance. Journal of Power Sources. 2004;138:120-36.

[21] Udagawa J, Aguiar P, Brandon NP. Hydrogen production through steam electrolysis: Control strategies for a cathode-supported intermediate temperature solid oxide electrolysis cell. Journal of Power Sources. 2008;180:354-64.

[22] Yee SK, Milanovic JV, Hughes FM. Overview and Comparative Analysis of Gas Turbine Models for System Stability Studies. IEEE Transactions on Power Systems. 2008;23:108-18.

[23] Kim JS, Powell KM, Edgar TF. Nonlinear model predictive control for a heavy-duty gas turbine power plant. 2013 American Control Conference2013. p. 2952-7.

[24] Tavakoli MRB, Vahidi B, Gawlik W. An Educational Guide to Extract the Parameters of Heavy Duty Gas Turbines Model in Dynamic Studies Based on Operational Data. IEEE Transactions on Power Systems. 2009;24:1366-74.

[25] Kunitomi K, Kurita A, Okamoto H, Tada Y, Ihara S, Pourbeik P, et al. Modeling frequency dependency of gas turbine output. Power Engineering Society Winter Meeting, 2001 IEEE2001. p. 678-83 vol.2.

[26] Mantzaris J, Vournas C. Modelling and stability of a single-shaft combined cycle power plant. International Journal of Thermodynamics. 2007;10:71-8.

[27] Kim JS. Modeling, Control, and Optimization of Combined Heat and Power Plants. Ph.D. dissertation. TX: Mcketta Department of Chemical Engineering, University of Texas at Austin; 2014.

[28] Rowen WI. Simplified mathematical representations of heavy-duty gas turbines. Journal of engineering for power. 1983;105:865-9.

[29] Rowen WI. Simplified mathematical representations of single shaft gas turbines in mechanical drive service. ASME 1992 International Gas Turbine and Aeroengine Congress and Exposition: American Society of Mechanical Engineers; 1992. p. V005T15A1-VT15A1.

[30] Kakimoto N, Baba K. Performance of gas turbine-based plants during frequency drops. IEEE Transactions on Power Systems. 2003;18:1110-5.

[31] Suzaki S, Kawata K, Sekoguchi M, Goto M. Combined cycle plant model for power system dynamic simulation study. TRANSACTIONS-INSTITUTE OF ELECTRICAL ENGINEERS OF JAPAN B. 2000;120:1146-52.

[32] Modelica Association. Modelica Conventions [Internet]. [updated 2013 Sep 23; cited 2016 Sep 26]. Available: http://simulationresearch.lbl.gov/modelica/releases/msl/Modelica%203.2.1/help/Modelica_UsersGuide_Conventions.html#Modelica.UsersGuide.Conventions.

APPENDIX A MODELICA CODE STANDARD

This section provides a checklist that should be used when contributing a new class (model, block, connector, function, package, etc.) to the libraries that comprise N-R HES models [9].

A.1 General

1. Follow the conventions of the MSL [32], which are as follows:

   Note, in the html documentation of any Modelica library, the headings "h1, h2, h3" should not be used, because they are utilized from the automatically generated documentation and headings. Additional headings in the html documentation should start with "h4."

   In the Modelica package, the following conventions are used:

   a. Comments and annotations always start with a capital letter, e.g.,
   ```
   parameter Real a = 1 "Arbitrary factor";.
   ```

   b. **Class and instance names** are usually written in upper and lower case letters, e.g., "ElectricCurrent". An underscore is only used at the end of a name to characterize a lower or upper index, e.g., "pin_a" may be rendered as "pin_a."

   c. **Class names** start always with an upper case letter.

   d. **Instance names**, i.e., names of component instances and of variables (with the exception of constants), start usually with a lower case letter with only a few exceptions if this is common sense (such as "T" for a temperature variable).

   e. **Constant names**, i.e., names of variables declared with the "constant" prefix, follow the usual naming conventions (= upper and lower case letters) and start usually with an upper case letter, e.g. UniformGravity, SteadyState.

   f. The two **connectors** of a domain that have identical declarations and different icons are usually distinguished by "_a", "_b" or "_p", "_n", e.g., Flange_a/Flange_b, HeatPort_a, HeatPort_b.

   g. The **instance name** of a component is always displayed in its icon (= text string "%name") in **blue color**. A connector class has the instance name definition in the diagram layer and not in the icon layer. **Parameter** values, e.g., resistance, mass, gear ratio, are displayed in the icon in **black color** in a smaller font size as the instance name.

   h. A **connector class** has the instance name definition in the diagram layer and not in the icon layer.

   i. A main package has usually the following subpackages:

      - **UsersGuide** containing an overall description of the library and how to use it.
      - **Examples** containing models demonstrating the usage of the library.
      - **Interfaces** containing connectors and partial models.
      - **Types** containing type, enumeration and choice definitions.
      - **BaseClasses** containing models, partial models, etc. that are not of interest to the user.

   In addition to the conventions of the MSL, the following conventions are used:

j. Names of models, blocks and packages should start with an upper-case letter and be a noun or a noun with a combination of adjectives and nouns. Use camel-case notation to combine multiple words, such as `HeatTransfer`.

k. Parameter and variables names are usually a character, such as `T` for temperature and `p` for pressure, or a combination of the first three characters of a word, such as `higPreSetPoi` for "high pressure set point".

l. Comments should be added to each class (package, model, function, etc.). The first character should be an upper case letter.

m. Where applicable, all variable, including protected variables, must have units.

2. All classes, with the exception of models within BaseClasses and constants, must have icons.

3. Examples, i.e., regression tests, should be in a directory such as Electrolysis.Examples.

4. Do not copy sections of code. Use object inheritance.

A.2 Type Declarations

1. Declare all public parameters before protected ones.

2. Declare variables and final parameters that are not of interest to users as protected.

3. Set default parameter values as follows:

   a. If a parameter value can range over a large region, do not provide a default value. Examples are nominal mass flow rates.

   b. If a parameter value does not vary significantly but need to be verified by the user, provide a default value by using its start attribute. For example, for a heat exchanger, use

   ```
   parameter Real eps(start=0.8, min=0, max=1, unit="1") "Heat exchanger effectiveness";.
   ```

   Do not use

   ```
   parameter Real eps=0.8(unit="1") "Heat exchanger effectiveness";
   ```

   as this can lead to errors that are difficult to detect if a modeler forgets to overwrite the default value of 0.8 with the actual value. The model will simulate, but gives wrong results due to unsuited parameter values and there will be no warning. On the other hand, using parameter Real eps(start=0.8) will give a warning and, hence, users can assign better values.

   c. If a parameter value can be precomputed based on other parameters, set its value to this equation. For example,

   ```
   parameter Medium.MassFlowRate m_flow_small(min=0) =
   1E-4*m_flow_nominal;.
   ```

   d. If a parameter value should not be changed by a user, use the final keyword. For example, use

   ```
   final parameter Modelica.SIunits.Frequency fn=60 "Nominal frequency";.
   ```

4. For parameters and variables, provide values for the min and max attribute where applicable. Be aware, that these bounds are not enforced by the simulator. If the min and max attribute are set, each violation of these bounds during the simulation may raise a warning. Compilers may allow to suppress these warnings. In Dymola, violation of bounds can be checked using

Advanced.AssertAllInsideMinMax=true;.

5. For any variable or parameter that may need to be solved numerically, provide a value for the start and nominal attribute.
6. Use types from Modelica.SIunits where possible.

A.3 Equations and Algorithms

1. Avoid events (i.e., discrete behaviors that are generated by conditional expressions) where possible.
2. If possible, only divide by quantities that cannot take on zero. For example, if x may take on zero, use y=x, not 1=y/x, as the second version indicates to a simulator that it is safe to divide by x.
3. Use the assert function to check for invalid values of parameters or variables. For example, use assert(phi>=0, "Relative humidity must not be negative.").
4. For computational efficiency, equations, shall were possible, be differentiable and have a continuous first derivative.
5. Avoid equations where the first derivative with respect to another variable is zero. For example, if x, y are variables, and x = f(y), avoid y = 0 for x<0 and y=x^2 otherwise. The reason is that if a simulator tries to solve 0=f(x), then any value of x <= 0 is a solution, which can cause instability in the solver. Note that this problem do not exist for constant functions, as their first derivate will replaced due to optimization within the solver.
6. Do not replace an equation with a constant that has a single value unless the derivative of the original equation is zero for this value. For example, if computing a pressure drop dp may involve computing a long equation, but one knows that the result is always zero if the volume flow rate V_flow is zero, one may be inclined to use a construct of the form dp = smooth(1, if V_flow == 0 then 0 else f(V_flow));. The problem with this formulation is that for V_flow=0, the derivative is dp/dV_flow = 0. However, the limit dp/dV_flow, as |V_flow| tends to zero, may be non-zero. Hence, the first derivative has a discontinuity at V_flow=0, which can cause a solver to fail to solve the equation because the smooth statement declared that the first derivative exists and is continuous.
7. Make sure that the derivatives of equations are bounded on compact sets. For example, instead of using y=sign(x) * sqrt(abs(x)), approximate the equation with a differentiable function that has a finite derivative near zero.

A.4 Package Order and Saving

1. Packages are first sorted alphabetically:
   Actuators
   Boilers
   Chillers
   HeatExchangers
2. After alphabetical sorting, the following packages, if they exist, are moved to the front:
   UsersGuide
   Examples
   and the following packages, if they exist, are moved to the end:
   Sources

```
Sensors
Media
Interfaces
Types
Data
Utilities (functions, records, etc.)
Icons
BaseClasses
```

3. When pushing any library to the Gitlab repository, make sure to save all the packages as "directories" as opposed to a "single file."

A.5 Documentation

1. Add a description string to all parameters and variables, including protected ones.
2. Group similar variables using the group and tab annotation. For example, use

```
parameter Modelica.SIunits.Time tau = 60
"Time constant at nominal flow" annotation (Dialog(group="Nominal
condition"));
```

or use

```
parameter Types.Dynamics substanceDynamics=energyDynamics
"Formulation of substance balance"
annotation(Evaluate=true, Dialog(tab = "Assumptions",
group="Dynamics"));.
```

3. Add model documentation to the info section. To document equations, use the format

```
<p>
The polynomial has the form
</p>
<p align=\"center\" style=\"font-style:italic;\">
y = a<sub>1</sub> + a<sub>2</sub> x + a<sub>3</sub> x<sup>2</sup> + ...,
</p>
<p>
where <i>a<sub>1</sub></i> is ...
```

To denote time derivatives, such as for mass flow rate, use

```
<code>m&#775;</code>.
```

To refer to parameters of the model, use the format

```
To linearize the equation, set <code>linearize=true</code>.
```

To format tables, use

```
<p>
<table summary=\"summary\" border=\"1\" cellspacing=\"0\" cellpadding=\"2\" style=\"border-
collapse:collapse;\">
<tr><th>Header 1</th>      <th>Header 2</th>     </tr>
<tr><td>Data 1</td>        <td>Data 2</td>       </tr>
</table>
</p>.
```

To include figures, place the figure into a directory in Electrolysis/Resources/Images/ that has the same name as the full package. For example, use

```
</p>
```

```
<p align=\"center\">
<img alt=\"Image\"
src=\"modelica://Electrolysis/Resources/Images/Electrolyzers/Electrolyzer.png\"/>
</p>
<p>.
```

To create new figures, put the source file for the figure, preferably in `svg` format, in the same directory as the `png` file. `svg` files can be created with http://inkscape.org/, which works on any operating system.

4. Add author information to the `revision` section.
5. Run a spell check.
6. Start headings with `<h4>`.
7. Add hyperlinks to other models using their full name. For example, use
   ```
   See <a href =\"modelica://Modelica.Fluid.Vessels.BaseClasses.VesselPortsData\">
   Fluid.Vessels.BaseClasses.VesselPortsData </a>.
   ```
8. To refer to names of parameters or variables in the documentation and revision sections, use the syntax `< code >...</ code >`. Do not use `<tt>...</tt>`.
9. Always use lower case html tags.

A.6 Functions

1. Use the `smoothOrder` annotation if a function is differentiable.

A.7 Regression Tests

1. Implement at least one regression test for each model and block, and run the regression tests. Regression tests should cover all branches of `if-then` constructs.

A.8 File Saving

1. Always use lower case html tags.

Appendix B COMPONENT MODELS THAT COMPRISE THE HTSE PLANT MODEL IN MODELICA

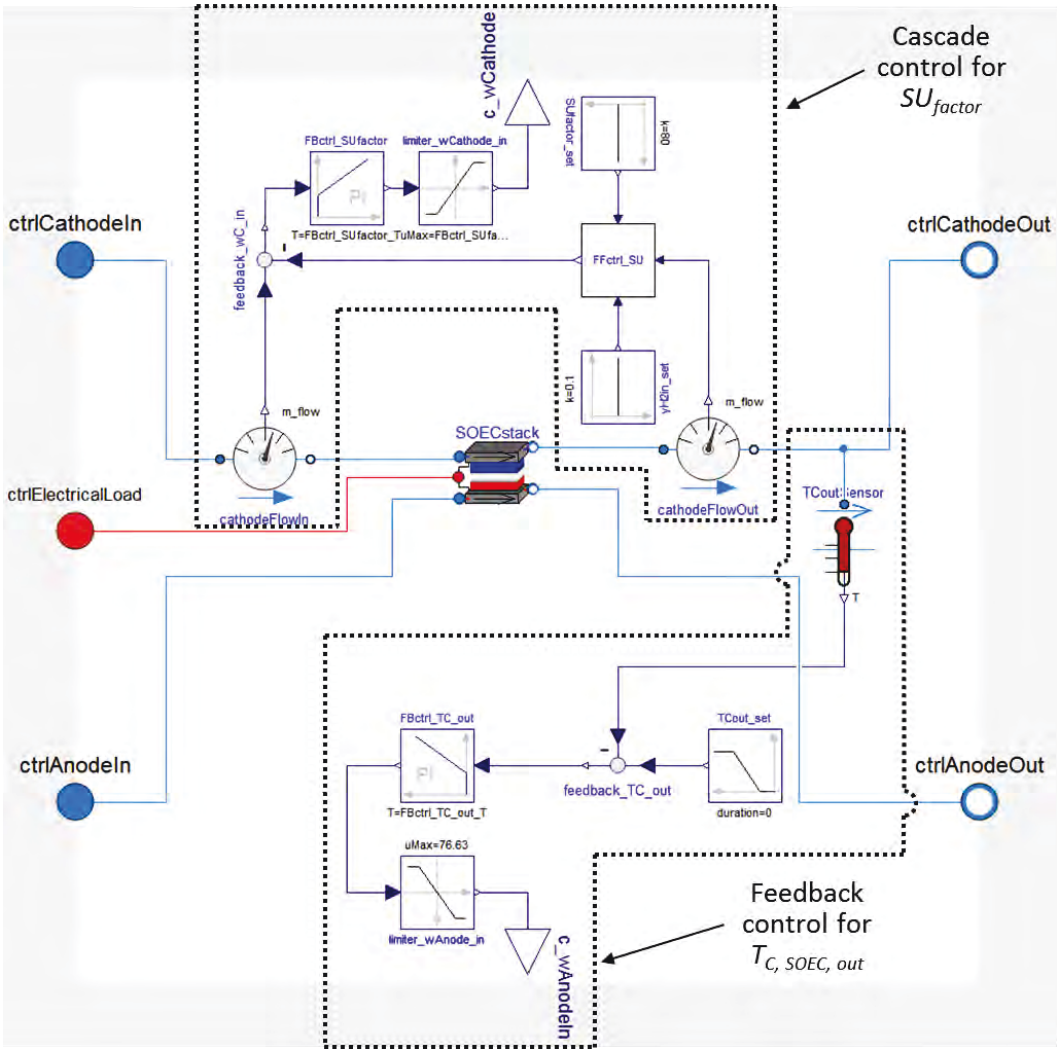

Figure B.1. Process model of SOEC stacks with regulatory control schemes.

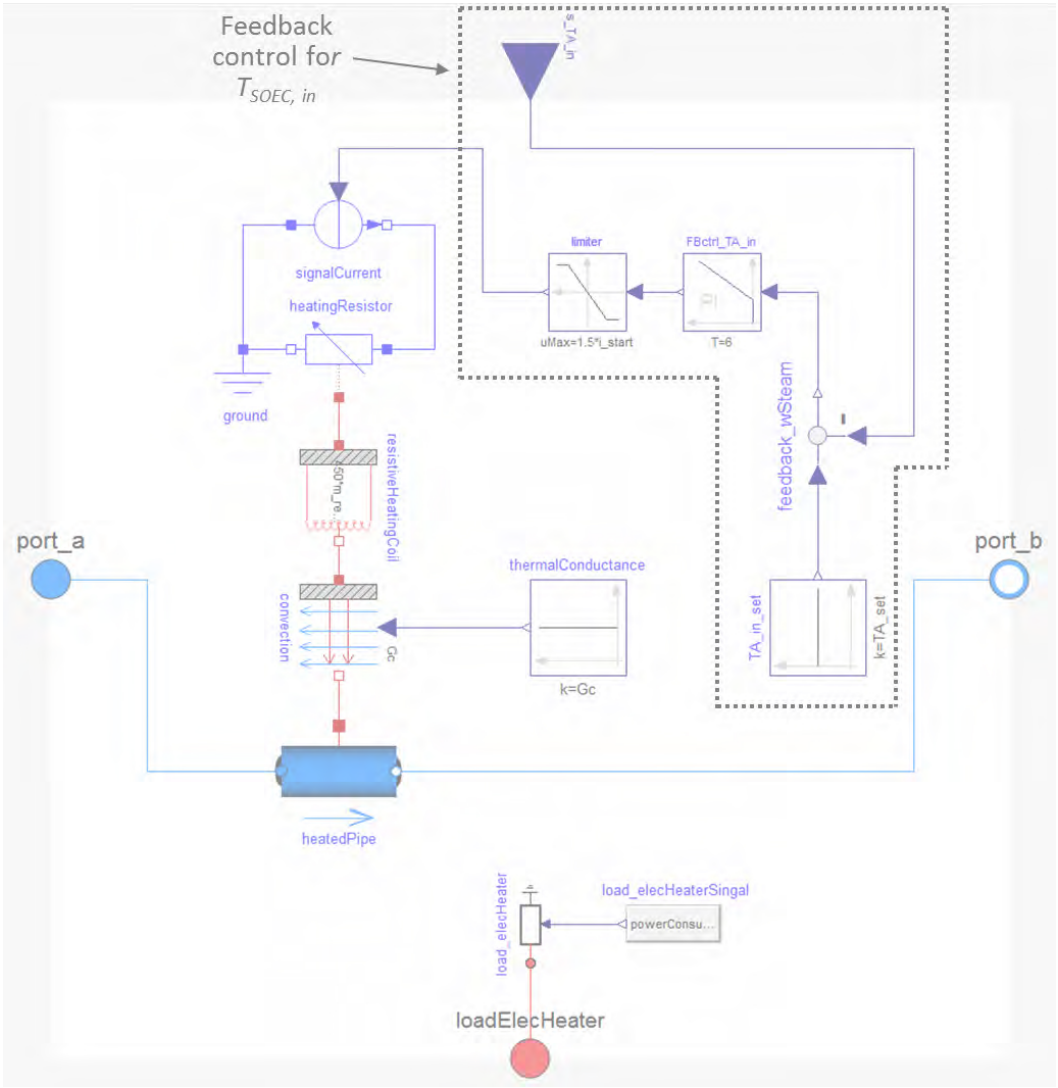

Figure B.2. Process model of an ETC with a regulatory control scheme.

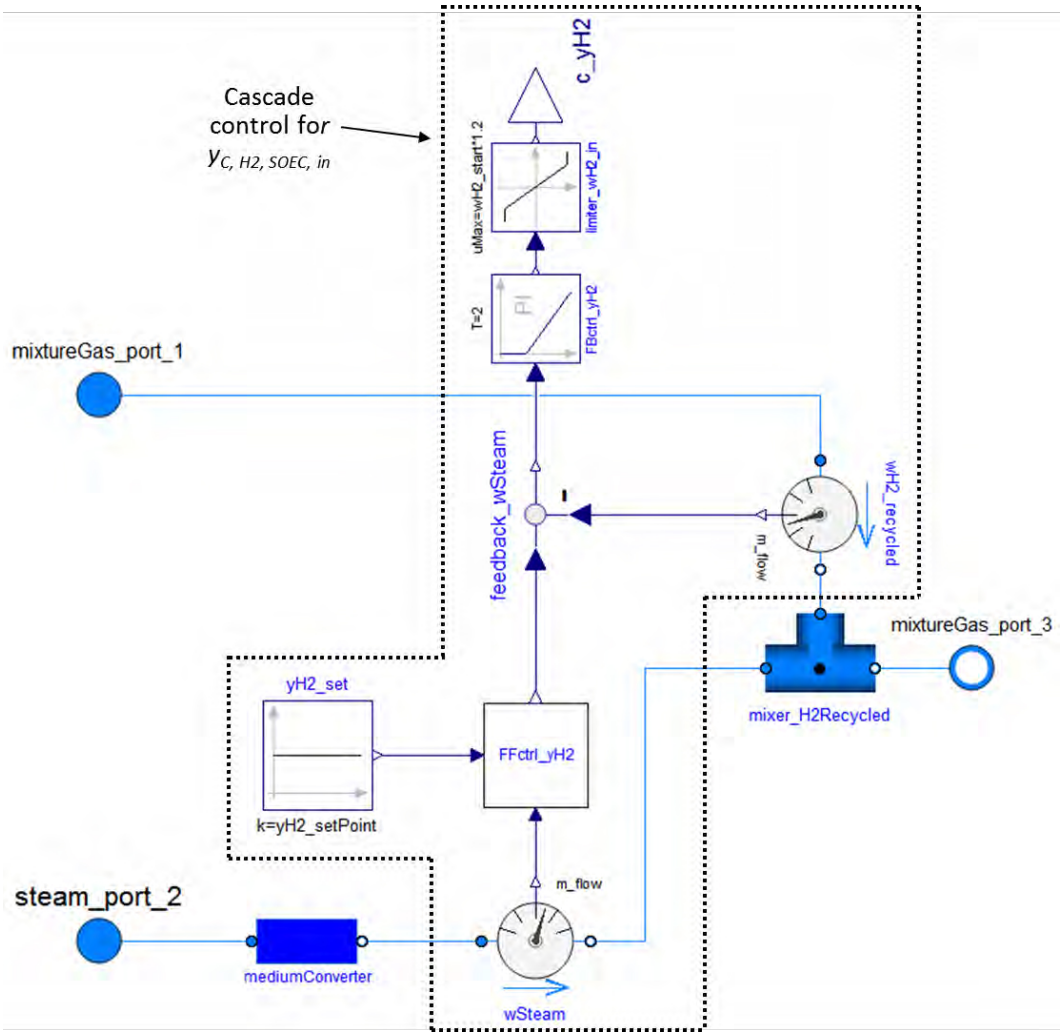

Figure B.3. Process model of a H_2/steam mixer with a regulatory control scheme.

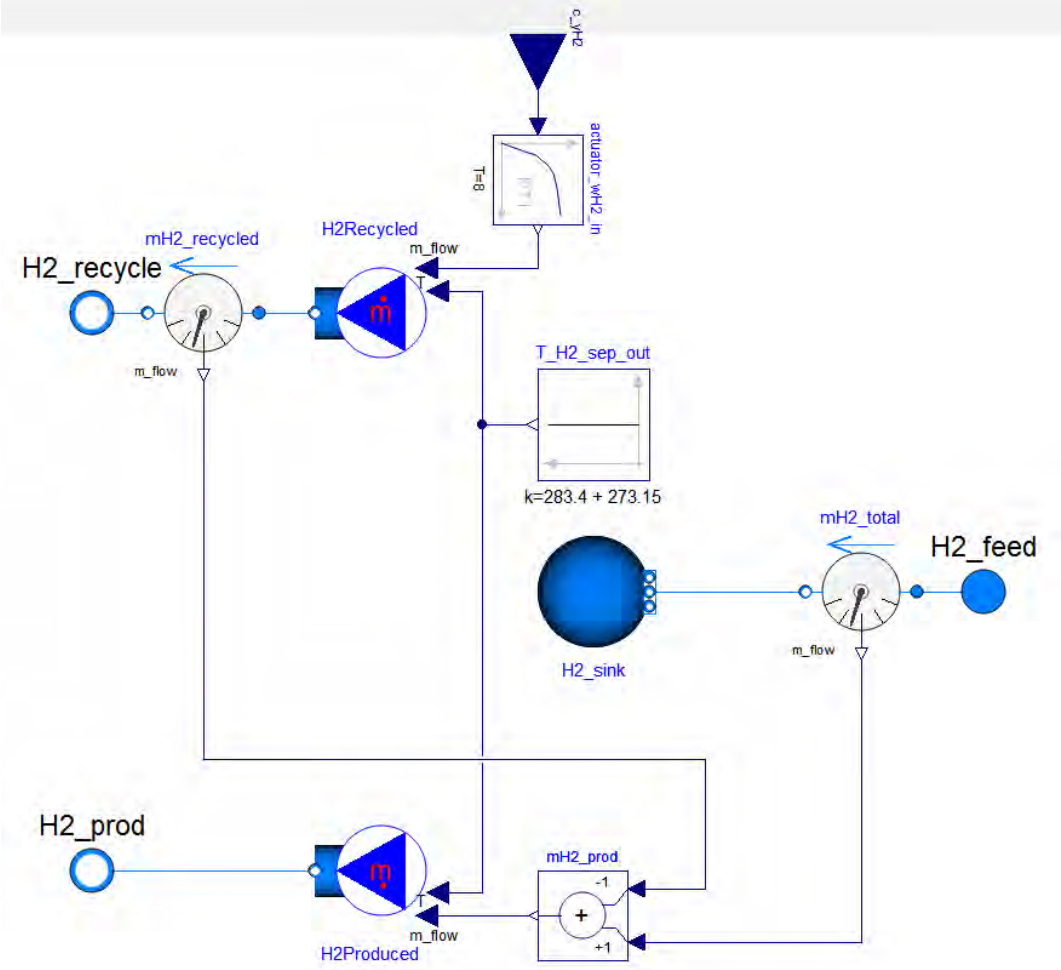

Figure B.4. Process model of a H_2 recycle loop.

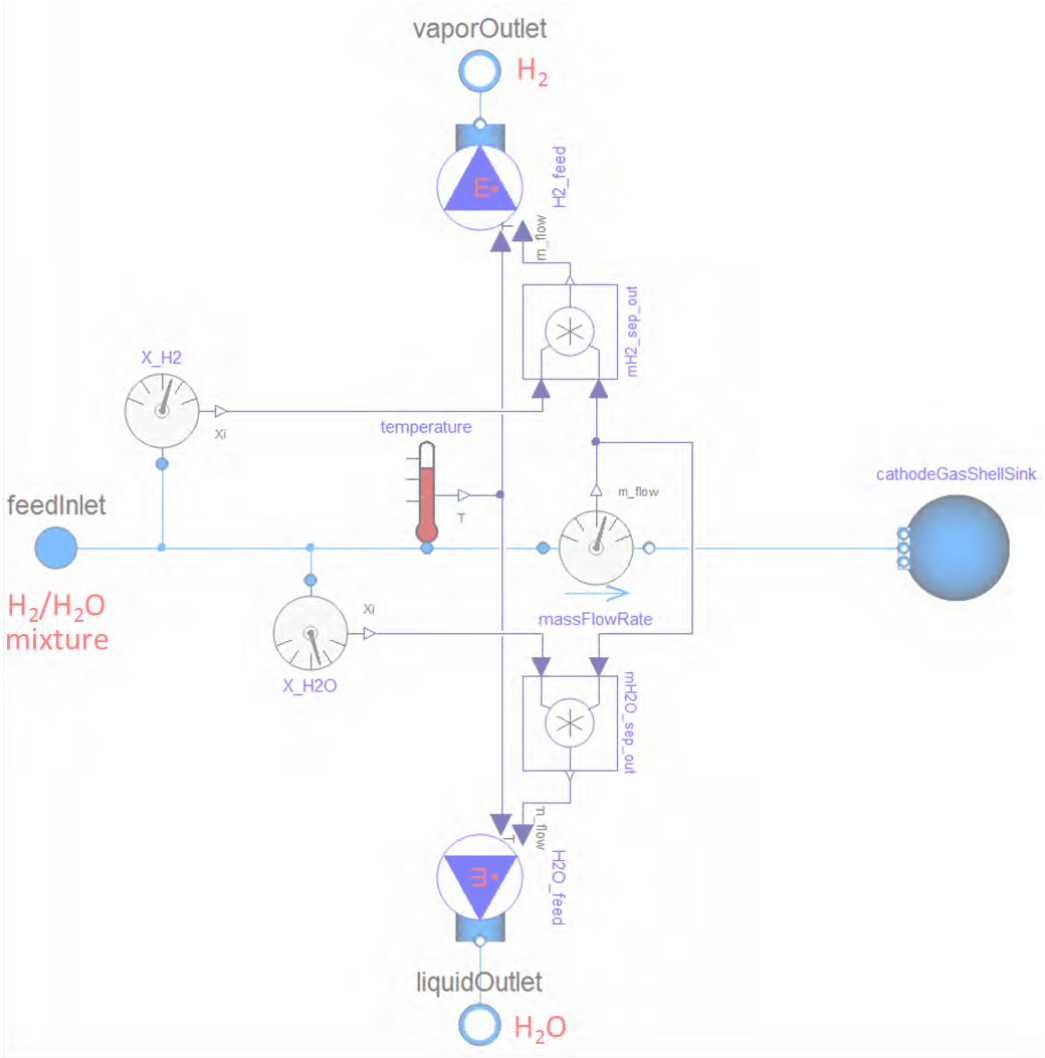

Figure B.5. Process model of a flash drum.

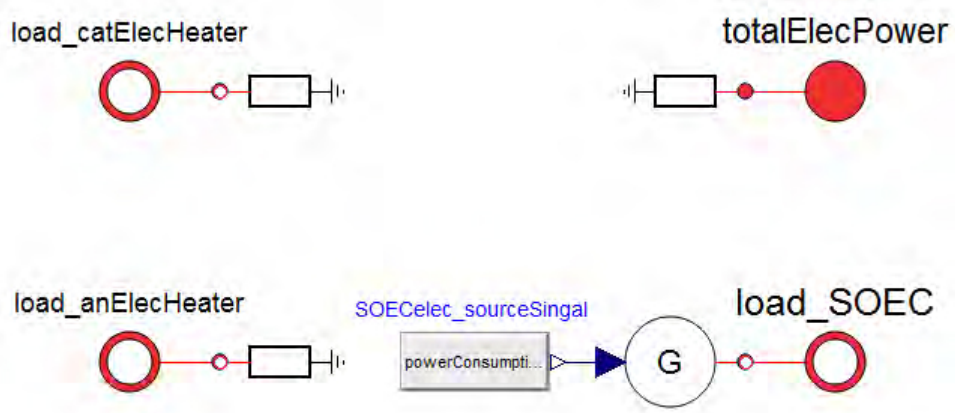

Figure B.6. Process model of a switchyard.